Field intercomparison of the gas/particle partitioning of oxygenated organics during the Southern Oxidant and Aerosol Study (SOAS)

By
Samantha Leigh Thompson
B.A., Carleton College, 2011

A thesis submitted to the
Faculty of the Graduate School of the
University of Colorado in partial fulfillment
of the requirement for the degree of
Masters of Chemistry
Department of Chemistry
2015

This Thesis entitled:
Field intercomparison of the gas/particle partitioning of oxygenated organics during the Southern Oxidant and Aerosol Study (SOAS)

Written by Samantha Leigh Thompson
has been approved for the Department of Chemistry

_____
Jose L Jimenez

_____
Paul Ziemann

Date _____

The final copy of this thesis has been examined by the signatories, and we find that both the content and the form meet acceptable presentation standards of scholarly work in the above mentioned discipline.

Thompson, Samantha Leigh (Masters, Chemistry)

Field intercomparison of the gas/particle partitioning of oxygenated organics during the Southern Oxidant and Aerosol Study (SOAS)

Thesis is directed by Professor Jose L Jimenez

We present results of the first intercomparison of real-time instruments for gas/particle partitioning of organic species. Four new instruments that directly measure gas/particle partitioning in near-real time were deployed at the Centreville, Alabama, Supersite of the Southern Oxidant Aerosol Study (SOAS) in the southeastern United States in the summer of 2013. Two were Filter Inlet for Gases and AEROsols High-Resolution Chemical Ionization Mass Spectrometers (FIGAERO-HRToF-CIMS) with acetate (A-CIMS) and iodide (I-CIMS) ionization sources, respectively, the third was a Thermal Desorption Aerosol GC-MS (TAG), and the fourth was a High-Resolution Thermal Desorption Proton-Transfer Reaction Mass Spectrometer (HR-TD-PTRMS). Signals from these instruments corresponding to elemental formulas of several organic acids are chosen for comparison of the measured gas/particle partitioning. Average partitioning of all common measured species shows a trend between TAG and A-CIMS with a slope of 1.86; between I-CIMS and A-CIMS with a slope of 1.68; and between PTRMS and A-CIMS and with a slope of 0.41. The comparison of time series show a substantial amount of scatter that is often averaged out in diurnal cycles to show similar diurnal trends, and absolute values that often agree within the error of the instruments. When the differences in partitioning observed among instruments are outside the estimated measurement errors, the causes may be due to measurement of different isomers resulting from differences in chemical sensitivities for different instruments, thermal decomposition during the heating cycles of the various instruments, or to other unidentified instrumental issues. There is some evidence for the presence of several isomers for several of the exact masses studied here from measurements using an ion mobility-CIMS at the field site. There is also evidence for the presence of several isomers and some thermal decomposition from the signal profiles of the heating cycles of the

CIMS instruments. This study shows promise for a measurement that was not feasible until very recently, while it also points to the difficulty of this measurement and its interpretation in a complex ambient environment, and the need for further improvements in measurement methodologies. Further intercomparisons under controlled laboratory conditions are recommended.

Acknowledgments

This research was partially supported by NSF AGS-1243354, DOE (BER/ASR) DE-SC0011105, and NOAA NA13OAR4310063. We are grateful to Annmarie Carlton, Karsten Baumann, and Eric Edgerton for their organization of the Centreville Supersite. We thank Julie Phillips of JILA for writing and editing support.

Contents

List of Tables

List of Figures

1. Introduction

Atmospheric aerosols have important effects on human health (Pope et al., 2009), visibility (Watson, 2002), and Earth's climate (Alley et al., 2007). Aerosols affect climate directly by scattering or absorbing light and indirectly by altering cloud brightness, lifetime, and precipitation (Alley et al., 2007). Recently, a long-term impact of aerosols on biogeochemical cycles has also been proposed with a radiative forcing comparable to that of the aerosol direct effect (Mahowald, 2011). Submicron particles are the most active climatically and most important for human health impact, and organic aerosols (OA) represents a substantial fraction of their mass (Kanakidou et al., 2005; Zhang et al., 2007; Jimenez et al., 2009).

OA can be classified into Primary OA (POA) that is directly emitted by both natural and anthropogenic sources and Secondary OA (SOA) that is formed by oxidation of gas-phase compounds followed by the gas-to-particle condensation of less volatile products (Pankow, 1994; Donahue et al., 2006; Jimenez et al., 2009) or by aqueous-phase chemistry (Lim et al., 2010; Ervens, 2015). Studies have demonstrated that a major fraction of OA is SOA across urban, rural and remote sites (de Gouw et al., n.d.; Hallquist et al., n.d.; Jimenez et al., n.d.). The formation, aging, chemical properties, and lifetime of OA are not well understood (Goldstein and Galbally, 2007; De Gouw and Jimenez, 2009; Hallquist et al., 2009), and these large uncertainties often lead to discrepancies between models and measurements of aerosol loading (de Gouw, 2005; Volkamer et al., 2006; Dzepina et al., 2009; Tsigaridis et al., 2014).

SOA has been long assumed to be semivolatile (Odum et al., 1996), however in the last few years several studies have suggested that some of the model/measurement discrepancies might be due to non-equilibrium gas/particle partitioning caused by kinetic limitations caused by the formation of glassy or semi-solid phases (Vaden et al., 2010, 2011; Virtanen et al., 2010). However, whether and when such limitations apply is currently controversial (Virtanen et al., 2010; Vaden et al., 2010, 2011; Shiraiwa et al., 2011; Perraud et al., 2012; Price et al., 2013; Renbaum-Wolff et al., 2013; Saleh et al., 2013; O'Brien et al., 2014; Yatavelli et al., 2014; Upshur et al., 2014; F.D. Lopez-Hilfiker et al., 2015; Yong Jie Li et al., 2015). To better understand and predict formation, growth, evolution, and losses of SOA, it is critical to understand gas/particle partitioning of organic species in the real atmosphere. Most studies to date

addressing the kinetic limitations to partitioning have been indirect methods and without chemical specificity. Accurate, direct, and fast time-resolution measurements of the gas/particle partitioning of key OA species are needed to resolve these discrepancies and clarify the representation of OA in atmospheric models.

Recently the direct in-situ measurement of the gas/particle partitioning of organic species and/or groups of species has become possible due to new instrumental developments (Holzinger et al., 2010b; Yatavelli and Thornton, 2010; Lopez-Hilfiker et al., 2013; Rollins et al., 2013; Isaacman et al., 2014). However these different measurements of particle-phase fractions have not been previously compared to our knowledge.

Because of their vapor pressure range, organic acids commonly partition between the gas and particle phases at typical atmospheric OA loading (~0.1-100 μg m^{-3}). Organic acids are abundant in the atmosphere (Chebbi and Carlier, 1996; Yatavelli et al., 2015) and are important oxidation products of anthropogenic and biogenic volatile organic carbon (VOC) species and contributors to SOA (Veres et al., 2011; Andrews et al., 2012; Vogel et al., 2013). Despite their ubiquity and importance, the gas/particle partitioning dynamics and equilibria of organic acids are still poorly uncharacterized.

Here, we compare results from four instruments that directly measured gas/particle partitioning of organic acids and related species with high time resolution for measurements collected at the ground supersite of the 2013 SOAS field study in the southeastern United States (Hu et al., 2015).

2. Instrumentation and Methods

Four instruments are compared in this study: Two filter inlet for gas and aerosol (FIGAERO) high-resolution–time-of-flight–chemical-ionization mass spectrometer (HRToF-CIMS) operated by different groups and with different ionization methods, a thermal-desorption aerosol gas chromatograph (TAG), and a high-resolution–thermal-desorption–proton-transfer-reaction mass spectrometer (HR-TD-PTRMS). All four instruments use thermal desorption to evaporate the particle-phase compounds before measurement. Details about each instrument can be found below and a diagram of the respective heating profiles experienced by a typical compound (desorbing at 100°C) is shown in Figure 1.

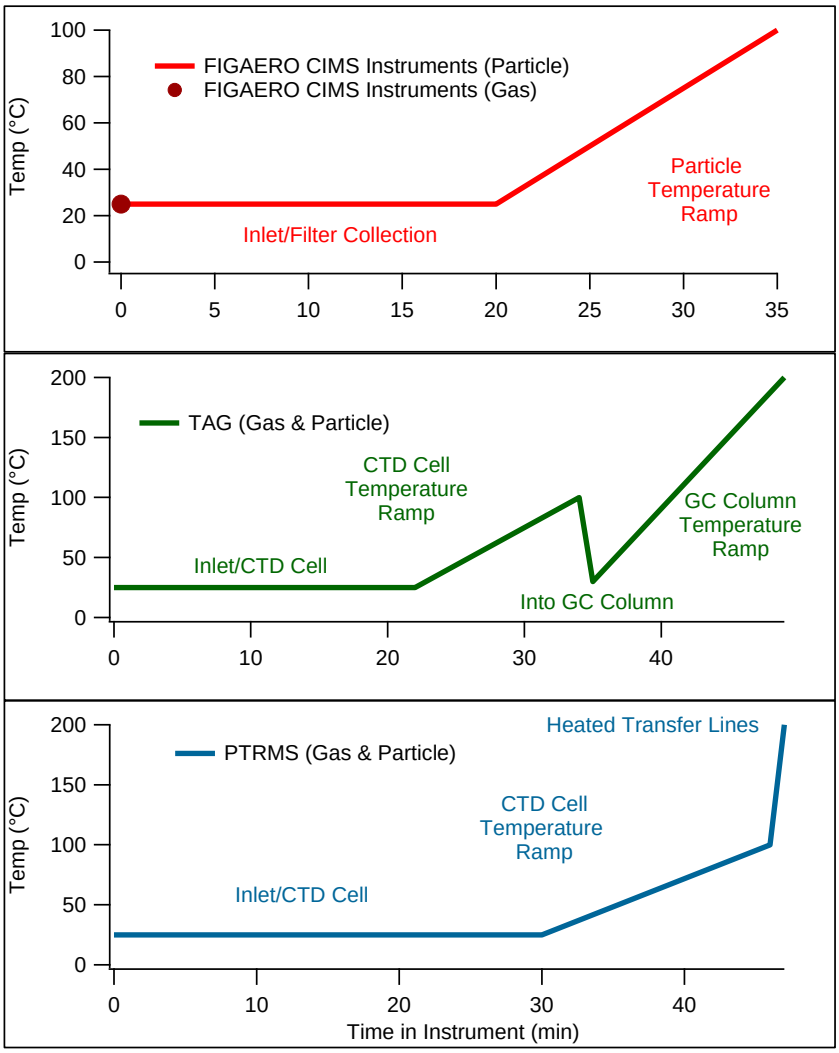

Figure 1. Schematic diagram of the temperature profiles that a typical compound would experience in the gas and particle phase in each instrument. The example compound is assumed to have a volatility such that it would thermally desorb at 100 ºC. The width of the thermal desorption curve (Lopez-Hilfiker et al., 2015) is ignored for the purposes of this diagram.

For the CIMS instruments the temperature ramp acts such that the molecules do not encounter a temperature greater than their thermal desorption temperature, decreasing the likelihood of thermal decomposition. In the PTRMS (which uses heated transfer lines) and the TAG (where a higher temperature is needed for a compound to flow quickly through the column) higher temperatures are experienced. That might increase the chances of thermal decomposition, although the residence times and materials that the species come into contact in the different instruments may also play a role. It has been

shown that some isoprene SOA oligomers do decompose in the I-CIMS at temperatures below 100°C (Lopez-Hilfiker et al., 2015) and the same is likely true in the other instruments. Note that no gas phase drying was applied to any instrument.

2.1. FIGAERO-HRToF-CIMS

Two of the instruments compared in this study use two versions of the same gas/particle inlet, followed by high-resolution chemical ionization mass spectrometric detection either with acetate (A-CIMS) or iodide (I-CIMS) reagent ions. The key components of this instrument are described in detail elsewhere (Yatavelli and Thornton, 2010; Lopez-Hilfiker et al., 2013; Yatavelli et al., 2014). Briefly, it is composed of three stages.

The first stage is the FIGAERO (Filter Inlet for Gases and AEROsols), an inlet designed to simultaneously sample atmospheric gases and aerosols on a semi-continuous basis (Lopez-Hilfiker et al., 2013). The inlet switches between different modes to measure gas and particle phase compounds. In the "sampling" mode, ambient air is drawn through the gas phase inlet and analyzed, while aerosols are simultaneously collected on a Tefllon filter. During the "desorption mode," both atmospheric sampling flows are still drawn through their inlets at the same rates (to avoid transient losses / sources in both inlets due to inlet adsorption / desorption if the flow was interrupted), but are bypassed directly into the pumps at the latest possible point. Meanwhile the aerosols are thermally desorbed off the filter and sampled into the instrument. Aerosol desorption is accomplished by heating ultra-high purity (UHP) nitrogen at a steady ramp rate of 17 ^{0}C per minute up to 200 ^{0}C while flowing it over the filter for 10 min. The nitrogen flow is then held at 200 ^{0}C for 20 additional min to increase the desororption of low volatility material and thus reduce any carry-over for the next collection / desorption cycle. Finally, room-temperature N_2 is passed over the filter for 5 min to cool the filter and its enclosure before initiating the next aerosol collection cycle. This entire cycle is repeated continuously every 55 minutes. Every 6th cycle is a "zero cycle," where UHP nitrogen is sampled through the gas inlet and a filter is placed in front of the particle phase inlet, using the same timing as described above for the ambient measurements, in order to regularly quantify the instrument and inlet backgrounds for both modes of operation.

The second stage of the instrument is the chemical ionization region (also known as ion-molecule reaction region, IMR). Chemical ionization (CI) enables sensitive and selective detection of targeted compounds. This region was set up with either acetate reagent ion or iodide reagent ion and are described in the following sections.

The third stage is the high-resolution–time-of-flight mass spectrometer, which rapidly (33 kHz averaged to 1 s) acquires the entire mass spectrum. The high-resolving power (R>4000 at *m/z* 300 in V ion-path mode as used here) of this stage allows for estimation of the elemental composition of many of the measured compounds (Decarlo et al., 2006; Yatavelli et al., 2012). Only the elemental composition of the analyte can be determined using this method, while structural isomers cannot be distinguished. In addition the instrument resolution is not sufficient to resolve all possible ions that could be present, which introduces some ambiguity in the analysis, especially for small peaks in a peak ensemble (Stark et al., 2015)

The A-CIMS is first described in detail, while the description of the I-CIMS summarizes the key differences with the A-CIMS.

2.1.1. Acetate CIMS

In the "sampling" mode, ambient air is drawn at 10 standard liters per minute (slpm) through a 6 m long 0.95 cm inner diameter Teflon tube, and then subsampled at the instrument entrance at 2 slpm, with a total inlet residence time of 2.5 s. Gas-phase species are analyzed continuously during the sampling phase. Simultaneously, aerosols are collected for 20 min on a Teflon filter at 10 slpm through a 0.95 cm inner diameter copper tube, also approximately 6 m in length, with an inlet residence time of 2.5 s. Both inlets sampled from approximately 6 meters off the ground.

In this source configuration, acetate ions [$CH_3C(O)O^-$] abstract a proton from organic acids, typically without (or with limited) fragmentation. This CI method is discussed in detail elsewhere (Veres et al., 2008). In the chemical ionization region, 2 slpm of sample gas is mixed with a 2 slpm flow containing the reagent ions. Acetate reagent ions are formed by flowing 2 slpm UHP nitrogen containing acetic anhydride (from bubbling the nitrogen through liquid acetic anhydride) through a Po-210 ionizer

(10 mCi). A residence time of ~100 ms in the CI region allows for the reagent ion / sample molecule reactions to proceed (~85 mbar). 0.5 slpm is then pulled into the mass spectrometer through an orifice, while the rest of the flow is exhausted through a pump. Due to the selective chemical ionization scheme used, most molecules detected are thought to be acids (Veres et al., 2008).

All data were processed using the custom Tofware software package (version 2.4.3; Tofwerk AG, Thun, Switzerland; Aerodyne Research Inc. Billerica, MA, USA (Stark et al., 2015) within Igor Pro (version 6.32; Wavemetrics, Inc., Lake Oswego, OR, USA).

2.1.2. I-CIMS

This instrument is conceptually identical to the one described above except for the reagent ion. This instrument uses I- as a reagent ion to selectively ionize relatively oxidized molecules. (Lee et al., 2014). The instrument was used with a FIGAERO collector and high-resolution mass spectrometer in the same way the A-CIMS was described above. The two FIGAERO collectors were built separately following the same design (by UW for the I-CIMS and by Aerodyne/Colorado for the A-CIMS).

2.2. TAG

A dual-cell Semivolatile Thermal desorption Aerosol Gas chromatograph (SV-TAG) with in-situ derivatization provided hourly measurement of functionalized semi- and low-volatile organic compounds in the gas- and particle-phases. A detailed description of this instrument has been provided elsewhere (Isaacman et al., 2014), and is only briefly summarized here. Sample air is drawn through an inlet and into two identical cells for collection and thermal desorption (CTD cells), which are collected at the same time then analyzed in series. The inlet is 2 stages: a “chimney” followed by a sub-sample line off the center stream. Air is pulled at ~200 slmp through a 38.7 cm wide cleaned steel duct (“chimney”) from an height of ~4 m above ground (residence time ~10-15 s). The TAG subsamples at 20 slpm (10 per cell) from the center stream through ~1 m of 0.95 cm ID clean stainless steel (SS) tubing. Each cell consists of a high-surface-area passivated SS metal fiber filter (Zhao et al., 2013) in a thermally controlled housing, which quantitatively collect gas and particle-phase compounds with a volatility as high as that of tetradecane ($C^* = 1e7\ \mu g\ m^{-3}$) (Zhao et al., 2013). During sample collection, one cell samples through a

400-channel cylindrical activated-carbon denuder (30 mm OD x 40.6 mm length; MAST Carbon) to remove gas-phase species. Simultaneous collection of total (undenuded) and particle-only (denuded) samples, followed by sequential analysis of the samples and subtraction to calculate gas concentrations, allows a direct calculation of gas/particle partitioning of the measured species. A typical duty cycle consists of 22 min of sampling on both cells, injection of standards (2 min), two-step desorption (12 min) and chromatographic analysis (14 min) of CTD1, and then desorption and analysis of CTD2 (14 min), while collection of the subsequent sample begins after exactly 60 min from the previous collection start. During analysis, samples are thermally desorbed into a helium purge flow saturated with derivatizing agent (MSTFA, N-Methyl-N-(trimethylsilyl)-trifluoroacetamide) in a two-step purge-and-trap method. Conversion of hydroxyl groups into silyl ethers and esters using MSTFA during the first stage of desorption allows quantitative analysis of highly polar compounds by gas chromatography/mass spectrometry (GC/MS). Analysis was performed using a custom-modified 7890A gas chromatograph (Agilent Technologies) equipped with a nonpolar column (20 m x 0.18 mm x 0.18 um, Rxi-5Sil MS; Restek) coupled to a 5975C unit-resolution quadrupole mass spectrometer (Agilent Technologies). Data was analyzed using custom TAG-specific software written in Igor Pro.

2.3. HR-TD-PTRMS

This instrument (hereinafter "PTRMS" for short) consists of a modified-commercial PTRMS instrument (PTR-TOF 8000, Ionicon Analytik GmbH, Innsbruck, Austria) with a high mass-resolution time-of-flight mass spectrometer (H-TOF, Tofwerk AG, Thun, Switzerland, same TOF analyzer used by A-CIMS and I-CIMS) with separate gas and aerosol inlets. We note that a PTRMS is technically an H_3O^+ CIMS but keep the former terminology as it is more commonly used in the literature. A custom-made sampler box contains 3 denuders in series to sample gas-phase species: 1st denuder DB-1 column, 0.53 mm x 5.0 μm for capturing Semivolatile Organic Compounds [SVOCs], 2nd denuder DB-1 column, 0.53 mm x 5.0 μm for capturing any leftover SVOCs, and 3rd denuder- activated carbon for capturing VOCs. SVOCs and VOCs are sampled through the denuder box for 30 minutes at a flow rate of 1 slpm. After sampling, a

reverse flow of UHP N_2 (70 sccm) was applied, and the PTRMS sampled the effluent N_2 from the denuder system containing the sampled molecules. The collection and analysis of particles have been described in detail by Holzinger et al. (2010a, 2010b). In a separate aerosol collection channel, particles in the size range 0.07–2 μm were collected by impaction on a Collection-Thermal-Desorption (CTD) cell. Aerosols collected from a total volume of 150–220 liters of air were desorbed from the CTD cell into a UHP N_2 flow of 7 mL min^{-1}. Thermally desorption increased the temperature in steps of 25°C min^{-1} for 16 min, up to a maximum of 350°C. The N_2 with the desorbed aerosol species was analyzed with the PTRMS. All transfer lines to the PTRMS were made of Sulfinert-coated (Restek) stainless steel and were heated continuously (200°C) to avoid re-condensation of evaporated organic material. Gas-phase background was measured every 9 hours by sampling ambient air through a platinum catalyst at 500°C, while aerosol background (sampling through a Teflon membrane filter, Zefluor 2.0 μm, Pall Corp.) was measured every other measurement cycle. A total of 16 measurement cycles were performed per day. Each cycle was completed in 90 min and included the analysis of the first CTD cell aerosol samples, second CTD cell aerosol samples (background), and the denuder gas samples. All data were processed using custom IDL software following Holzinger et al. (2010b).

2.4. Gas/particle partitioning calculations.

All gas/particle partitioning measurements are expressed as fractions of a given species (i) in the particle phase ($F_{p,i}$), calculated as the ratio of the measured particle-phase concentration to the measured total concentration (gas plus particle) after subtraction of any instrument backgrounds, i.e.:

$$F_{p,i} = \frac{Particle}{(Gas+Particle)} . \quad (1)$$

2.5. Uncertainty Estimation

Measurement uncertainties were estimated for each instrument based on its particular measurement method. Note that the estimated errors do not include uncharacterized errors that may be factors such as interfering isotopes, decomposition, oligomer interference, or various sampling artifacts.

For A-CIMS and I-CIMS, the total uncertainty is calculated as the combination of the estimated accuracy and precision:

$$\sigma_{Fp} = \sqrt{accuracy^2 + precision^2}\ . \quad (2)$$

Particle and gas-phase signals are calculated for the CIMS instruments as

$$Concentration = (Signal_{raw} - Background) * Sensitivity\ . \quad (3)$$

Each of the three components (signal, background, and sensitivity, for the gas and particle phase measurements) has an accuracy and a precision, resulting in up to 12 components contributing to the overall F_p uncertainty. The estimation methods for each of these 12 components can be found in the supplemental information Table 1.

	Calculated	A-CIMS	I-CIMS
Particle Phase Errors			
Particle Signal Accuracy	From particle phase calibration. Repeats of same concentration	9.1%	12%
Particle Background Accuracy		N/A	5%
Particle Sensitivity Accuracy		N/A	12%
Particle Signal Precision	Standard deviation of steady particle phase signal	6.24	10%
Particle Background Precision	Standard deviation of background signals	20%	2.5%
Particle Sensitivity Precision	From repeated calibrations of a compound	24%	20%
Gas Phase Errors			
Gas Signal Accuracy	From gas phase calibration. Repeats of same concentration	4.1%	17%
Gas Background Accuracy		N/A	40%
Gas Sensitivity Accuracy		N/A	12%
Gas Signal Precision	Standard deviation of steady signal	22%	1%

Gas Background Precision	Standard deviation of background signals	5.5%	12%
Gas Sensitivity Precision	From repeated calibration of a compound	20%	10%

Table 1. Summary of the components in the error calculation for the two FIGAERO CIMS instruments.

All estimated uncertainties (shown as error bars) are 1σ. Further information on the CIMS error estimates can be found in Lopez-Hilfiker et al. (2014).

All F_p values from the TAG have an estimated total relative uncertainty of ±15% (1σ). Further information on the estimation of this value can be found in Isaacman et al. (2014). All PTRMS F_p values have an estimated total relative uncertainty of ±30% (1σ). Further information on the estimation of this value can be found in (Holzinger et al., 2010b).

2.6. Ion Mobility Nitrate CIMS

Ion mobility-mass spectrometry (Eiceman and Karpas, 2010) measurements were obtained from a drift-tube ion mobility spectrometer coupled to a high-resolution time-of-flight mass spectrometer (IMS-TOF; Tofwerk AG, Thun, Switzerland). The instrument has been described in detail in previous publications (Kaplan et al., 2010; Zhang et al., 2014). The IMS-TOF was deployed during SOAS with a custom-built nitrate-ion (NO_3^-) chemical ionization source initiated with an X-ray ionizer (Hamamatsu Photonics, Hamamatsu, Japan). Data were post-processed and analyzed using the Tofware IMS data analysis package for Igor Pro. Additional results from the IMS-TOF at the SOAS site will be described in a forthcoming publication.

2.7. Modeling

Gas/particle partitioning was also modelled using equilibrium partitioning theory for absorptive partitioning into the organic aerosol phase (Pankow, 1994; Donahue et al., 2006) with the following equations:

$$F_{p,i} = \left(1 + \frac{C_i^*}{C_{OA}}\right)^{-1} \quad (4)$$

$$C_i^* = \frac{M_i 10^6 \zeta_i P_i}{760RT} \quad (5)$$

Where *i* represents a given species, F_p is fraction in the particle phase, C_i* is the saturation mass concentration (μg m^{-3}), C_{OA} is the organic aerosol mass concentration (μg m^{-3}), M_i is the molecular weight (g mol^{-1}), ζ is the activity coefficient (assumed = 1), P_i is the pure component liquid vapor pressure (Torr), *R* is the universal gas constant (8.2×10^{-5} m^3 atm K^{-1} mol^{-1}), and *T* is the ambient temperature (K). Values for C* can be found in Table S1.

The partitioning of the compounds to the aqueous phase was also estimated. Using an average aerosol liquid water content of 15 μg m^{-3} (Nguyen et al., 2014) and literature values for Henry's Law Constants (Compernolle and Müller, 2013) of 1.3×10^9 for hydroxy glutaric acid, 1.4×10^8 for pinic acid and 202 (all in M atm^{-1}) for pinonic acid we estimated partitioning fractions to the aerosol liquid water of 0.32, 0.05 and 7×10^{-8} respectively. So for hydroxy glutaric acid, partitioning to the aqueous phase may be playing a significant role, while it plays less of a role for pinic acid and is not playing a role at all for pinonic acid. This will be discussed in detail later.

2.8. SOAS Field Study

All the instruments were deployed during the SOAS field study at the ground-based supersite in Centreville, Alabama, in the summer of 2013. The study is described in detail elsewhere (Hu et al., 2015). We selected a time period for intercomparisons of about nine days, 17-25 June, 2013, during which all four instruments were sampling simultaneously. Appendix B shows the average diurnal cycles of temperature, relative humidity, and organic aerosol concentration. Temperatures ranged from 22-28ºC, RH ranged from 70-100% with sporadic precipitation, and organic aerosol ranging from 4-9 μg m^{-3} on average.

3. Results and Discussion

The results are separated into two sections. The first section compares the results from A-CIMS, I-CIMS, and TAG. The second compares the A-CIMS and the PTRMS. This structure was chosen because

the TAG and I-CIMS did not measure any common compounds with the PTRMS and thus a comparison between those instrument pairs is not possible. A table of all the compounds discussed in this paper and their elemental formulas can be found in the supplementary information in Appendix A.

3.1. Comparison of A-CIMS, I-CIMS and TAG

Three acids were measured by all three instruments. These were the only three acids that were positively identified with the TAG, that were also seen by the A-CIMS and I-CIMS. The three compounds span a large range of F_p values (from all 3 instruments), from 0.04 to 0.88. We first present a summary of the comparison for the averages of the whole period sample, followed by a detailed time-resolved analysis of the comparisons for individual compounds.

3.1.1. Comparison of Whole-Period Averages

The average measured F_p for the three common species and the entire sampling period are compared in Figure 2a.

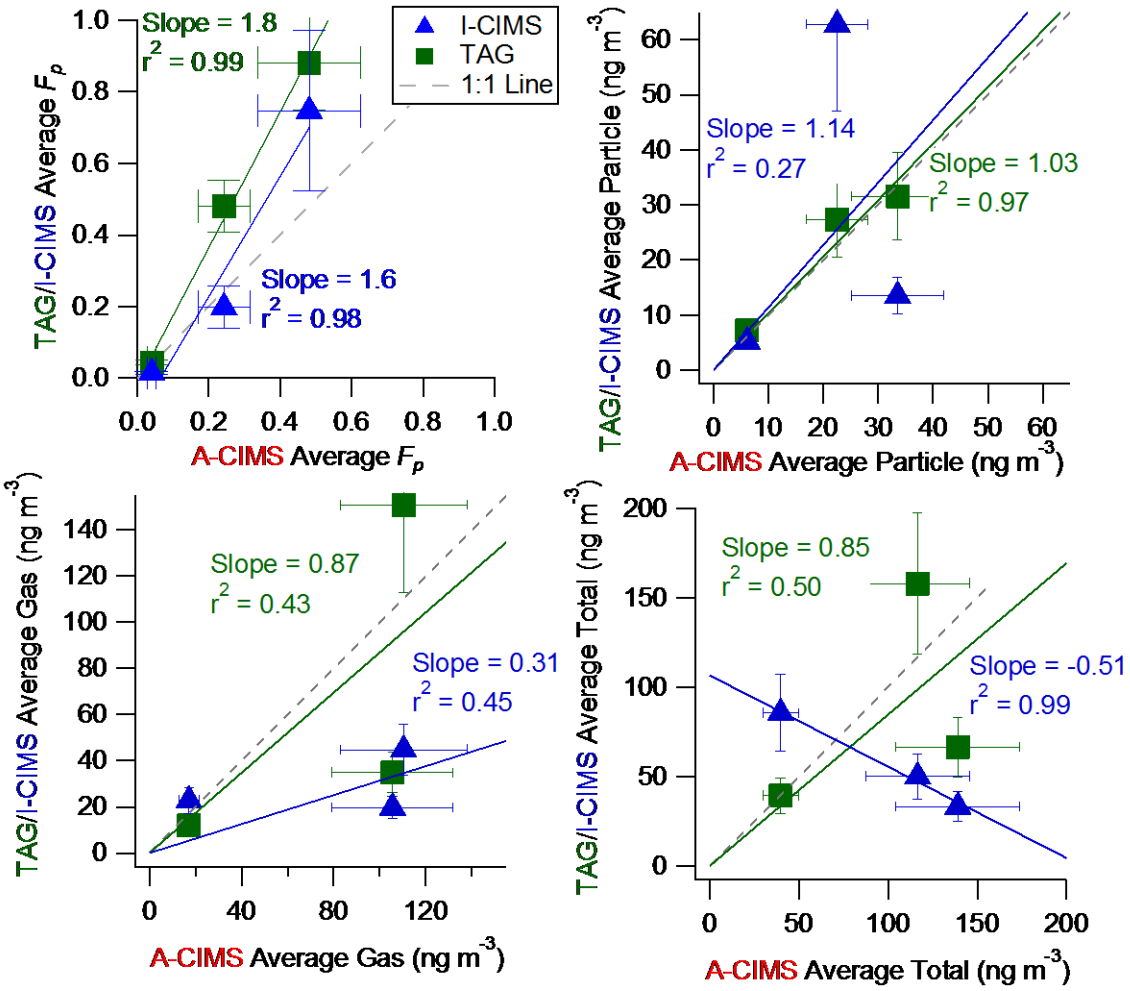

Figure 2. Scatter plots of the average measured F_p (a), particle concentration (b), gas concentration (c) and total concentration (d) over the entire overlap period from TAG and I-CIMS vs. A-CIMS. Each point represents one compound.

All three instruments show a consistent trend across across the entire range of possible F_p values (0–1). The average partitioning values show slopes of 1.86 (r^2=0.99) and 1.68 (r^2=0.98) for TAG/A-CIMS and I-CIMS/A-CIMS, respectively. The I-CIMS measures consistently higher F_p values than the A-CIMS, but within the estimated uncertainties of the measurements, while the TAG measures higher values than the A-CIMS than can not be explained by the estimated uncertainties. Note that the estimated errors do not include uncharacterized errors that may be factors such as interfering isotopes, decomposition, oligomer interference, or various sampling artifacts discussed above. All instruments report gas, particle, and total concentrations of the same order of magnitude, typically of tens of ng m^{-3} for

the species studied. The absolute concentrations measured show varying degrees of agreement and correlation. The TAG and A-CIMS show excellent agreement for the average particle phase concentrations where the F_p values did not (Fig. 2b), while the gas-phase measurements show more scatter, primarily due to a x2.5 lower pinic acid gas-phase concentration in TAG vs. A-CIMS (Fig. 2c). I-CIMS vs. A-CIMS particle phase concentrations are of the same order but show significant scatter, while the gas phase concentrations are much lower in the I-CIMS than in the A-CIMS for the two lower volatility species. For the total concentrations an anti-correlation is observed. Thus the study-average comparison shows mixed results: concentrations are of the same order and F_p values show high correlation, but there are substantial disagreements in some of the concentrations. In the next 3 sections we explore the three comparisons at high time resolution. The time resolution used here is one hour, which is the duty cycle of most of the instruments.

3.1.2. Detailed Comparisons for Pinonic Acid

All three instruments measured $C_{10}H_{16}O_3$ ("pinonic acid," where the quotes indicate some ambiguity on the true species detected, as discussed below). The CIMSs identified it via its elemental formula, and with the TAG by a match of retention time and mass spectrum with a standard. We note that the CIMS measurements may also include other species of the same elemental composition, and the same applies to other species intercompared and discussed below. There are many possible isomers for this elemental formula, several of which are acids (measurable by the A-CIMS) and other oxidized compounds (potentially measurable by the I-CIMS). Pinonic acid is an oxidation product of α-pinene (Szmigielski et al., 2007) and so its presence is expected at this field site where α-pinene was abundant. Figure 3 shows the time series, scatter plot, and diurnal cycle of F_p (top), particle phase concentration (second row), gas phase concentration (third row) and total (particle + gas) concentration (bottom). This species was mostly in the gas phase with an F_p below 7%, according to all instruments.

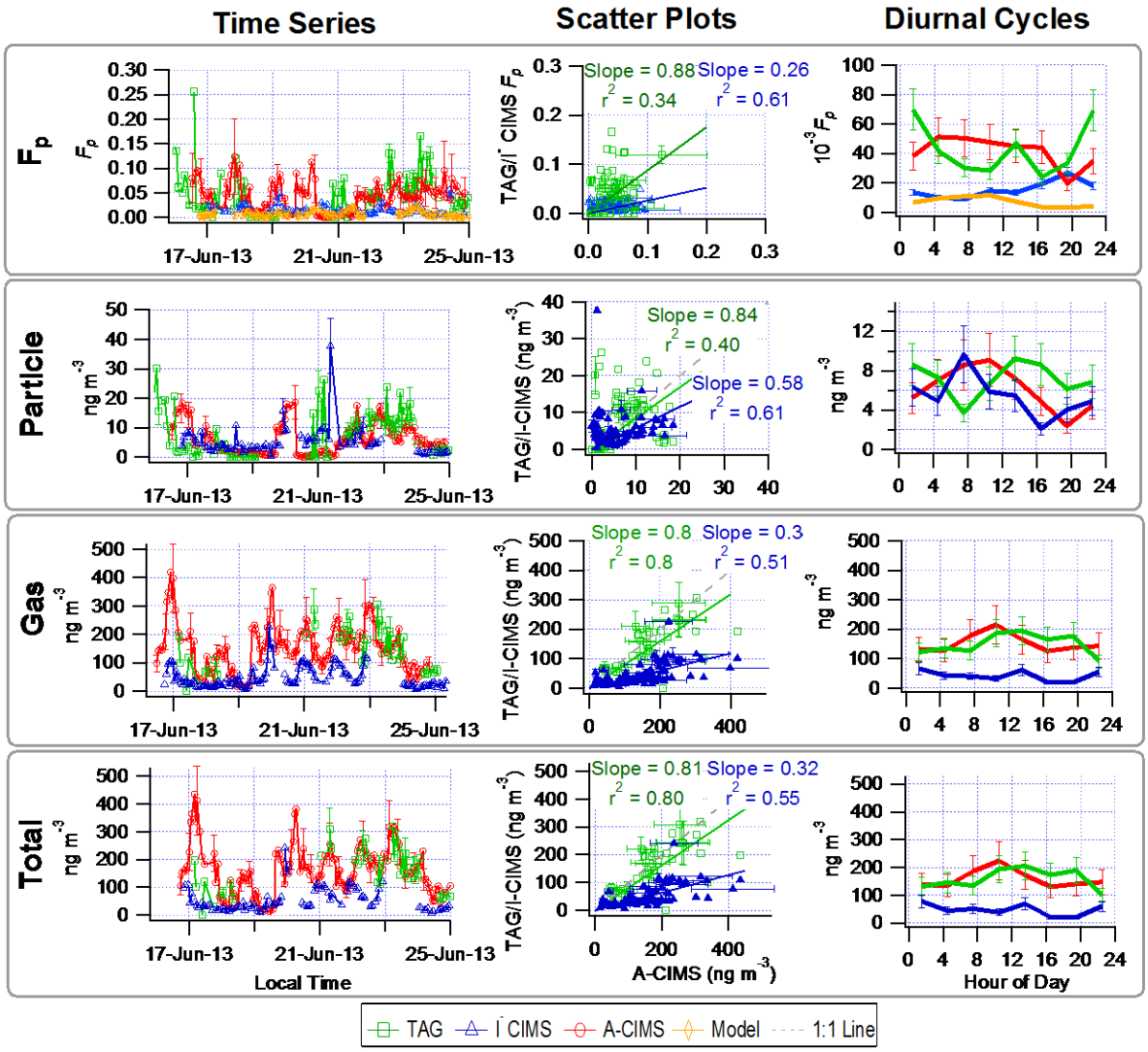

Figure 3. Time series (left), scatter plots (center) and diurnal cycles (right) of the measured particle-phase fraction (F_p, top row), and particle phase (2nd row), gas phase (3rd row) and total concentrations (bottom row) for $C_{10}H_{16}O_3$ ("pinonic acid") for the A-CIMS, I-CIMS, and TAG. Error bars represent estimated instrumental uncertainties as described in section 2.5. Modeled values for F_p are also shown in the top row. Regressions are fixed through origin and done with ODR.

A substantial degree of scatter is observed in all comparisons, with R^2 in the range 0.34-0.80. The TAG and A-CIMS show stronger agreement for concentrations. In contrast, the I-CIMS tends to report lower concentrations than the A-CIMS, with lower correlation than TAG/A-CIMS for some parameters and higher for others. Averaging the individual data points into diurnal cycles results in smooth variations in most cases, with similar trends as already discussed. All the instruments are consistent with the absorptive partitioning model predictions (yellow), showing this species to be almost entirely in the gas phase,

though none are as low as the model and all show different diurnal cycles than predicted. There is a substantial uncertainty in the model predictions due to large uncertainties in vapor pressures (Bilde et al., 2015), which could account for some of the model / measurement differences. Partitioning to the aqueous phase predicts an even lower value by several orders of magnitude.

There are many possible reasons for the disagreement between the instruments. The individual points display substantial scatter that may be partially due to noise in the measurements. It may also be that the CIMS instruments are measuring different isomers with the same elemental composition, whose concentration ratio can also vary with time. Note that it is also possible that the CIMS instruments are measuring the same several species, but with different relative sensitivities, which would result in different convolutions of the species time series. The instruments have significant differences in their thermal desorption profiles (Fig. 1). In particular the TAG heats the particle-phase compounds prior to analysis to much higher temperatures than needed for thermal desorption temperature; and the TAG heats the gas-phase species while this is not the case on the CIMS. The TAG also subjects the compounds to two heat ramps compared to one for the CIMS. In all instruments there may be false particle phase signal due to larger molecules (oligomers) decomposing at higher temperatures into the detected smaller species (monomers), leading to a larger measured F_p than would be expected given the measured species composition (Lopez-Hilfiker et al., 2015). There may also be some thermal decomposition of the compound of interest for the CIMS during the particle analysis but not the gas-phase analysis, leading to lower measured F_p. The extent of thermal decomposition in each instrument will depend on the species, temperature time profiles, as well as the materials that the species comes into contact. Although the stronger heating described above might indicate that the TAG might have higher thermal decomposition, at present it is not possible to predict relative trends between the instruments owing to their many differences. Some insight into the thermal decomposition issue can be obtained from the CIMS thermograms, and this is discussed below. We recommend future laboratory studies to characterize the response of each instrument to the species of interest.

To further investigate these discrepancies, two deeper aspects of the A-CIMS measurements were investigated. Figure 4a shows the high resolution peak fitting used to identify this elemental formula at *m/z* 183 in the A-CIMS.

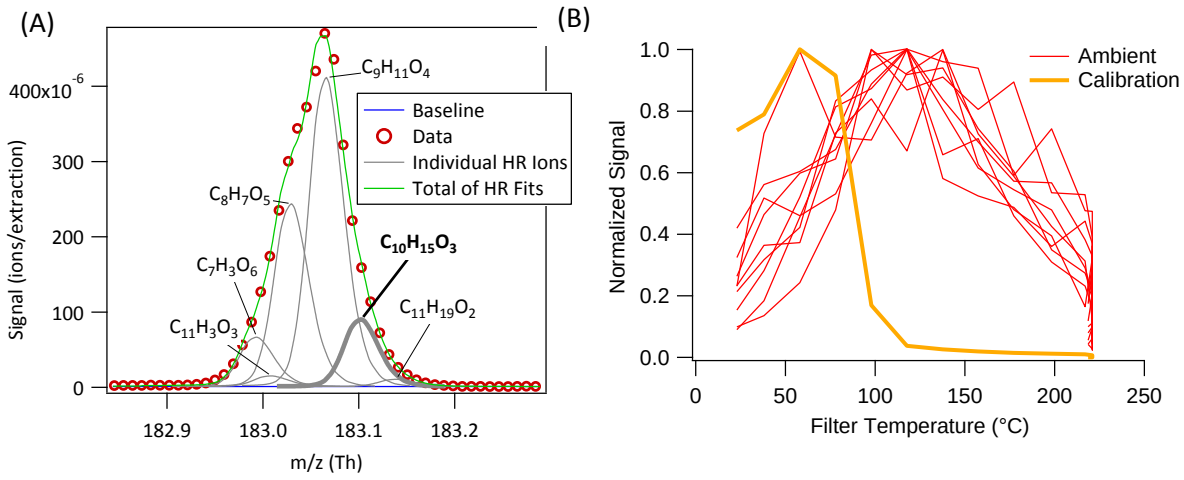

Figure 4. Additional information for the formula $C_{10}H_{16}O_3$ (pinonic acid and isomers, measured in the A-CIMS as $C_{10}H_{15}O_3^-$). (a) High resolution signal fits averaged over one day. Formula under study is in bold. (b) Signal vs temperature for several ambient heating cycles during SOAS (red) as the FIGAERO filter is slowly heated (see text for details). Heating cycles selected at random over the 10 days of the study and encompass a range of days and time of day. A calibration thermogram with a mixture of acids is shown in yellow. Calibrations carried out in a mixture of 50 compounds of varying volatility with each individual compound making up to 4% of the total deposited on the filter, but the ambient aerosol will have a different composition and also contains substantial fractions of inorganic species that were not present in the calibration mixture. The amount deposited was kept close to ambient amounts.

The peak under study ($C_{10}H_{15}O_3^-$) is a part of a much larger peak, making its area more difficult to quantify, even though the group of peaks is well fit. Figure 4b shows several thermal desorption profiles from the A-CIMS instrument for the signal measured at the *m/z* with formula $C_{10}H_{15}O_3^-$ (pinonic acid), along with an example calibration profile of pinonic acid. The ambient thermal desorption profiles were randomly selected and cover a range of different times of day over the 10 days being compared in this study. Calibrations were conducted by deposition of a known amount of pinonic acid (in solution) onto the FIGAERO filter. See figure caption for more details on the calibration mixture. The calibration compound desorbs from the filter at much lower temperatures (~60º C), than the ambient data (~120º C).

It is possible that the ambient signal is not dominated by pinonic acid, but either an isomer with a lower vapor pressure (which would cause it to desorb from the filter at higher temperatures), or more likely the breakdown of a larger molecule or oligomer detected at this elemental formula. It is also possible that the difference is due to different matrix effects between the simple calibration mixture and the complex ambient aerosol. These complex aspects of the detection process, which will also present themselves in different ways in the other instruments, make it difficult to reach a firm conclusion for the reasons of the disagreements observed.

3.1.3. Detailed Comparisons for Pinic Acid

The partitioning values for $C_9H_{14}O_4$ ("pinic acid") indicate some level of agreement in the time series, shown in Figure 5, with regression slopes of 0.7 (r^2=0.31) between I-CIMS/A-CIMS and 1.75 (r^2=0.38) and TAG/A-CIMS, although neither is well correlated.

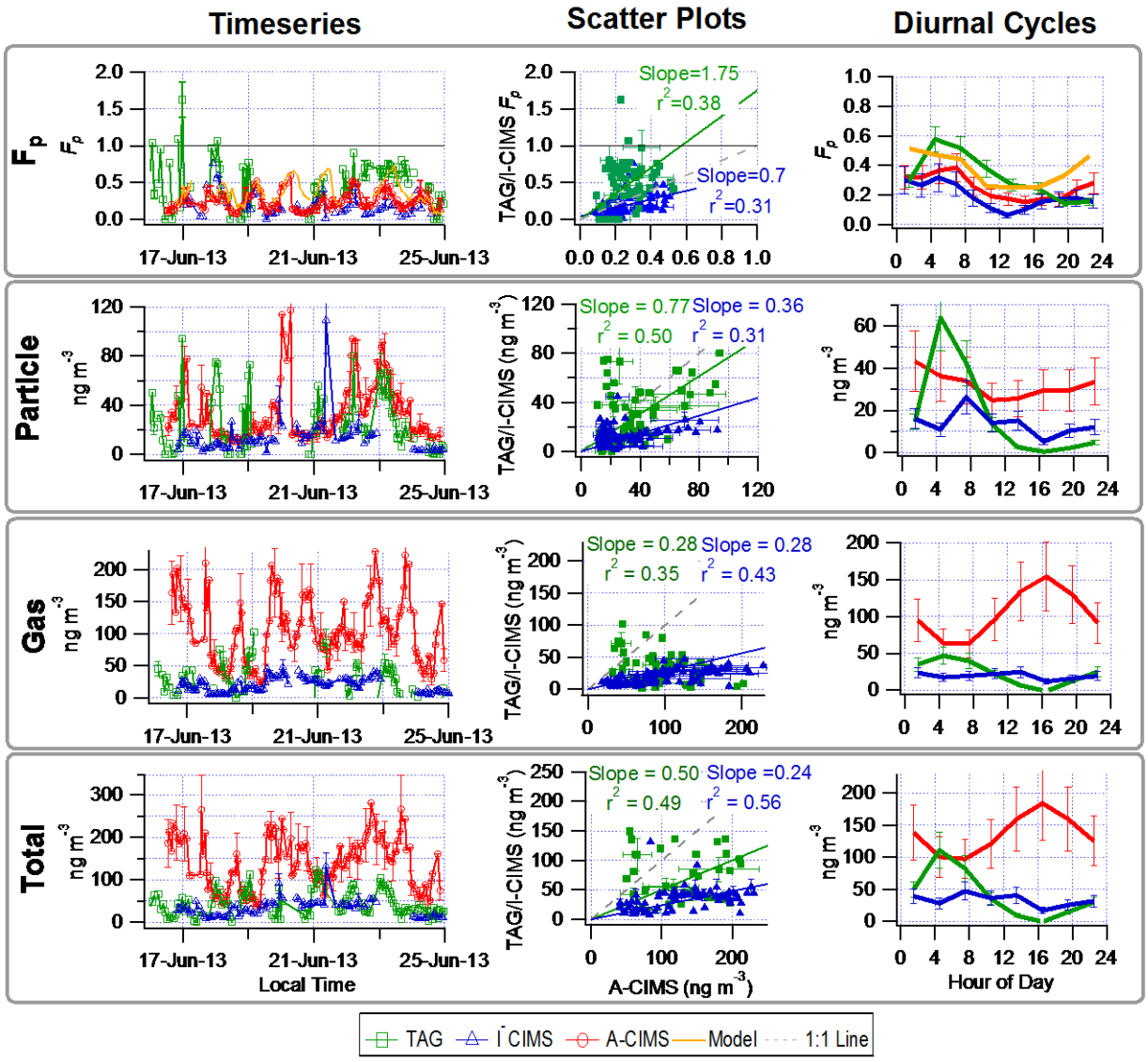

Figure 5. Time series (left), scatter plots (center) and diurnal cycles (right) of the measured gas/particle partitioning (F_p top row), particle phase (2nd row), gas phase (3rd row) and total concentration (bottom row) for $C_9H_{14}O_4$ ("pinic acid") the acetate (A-CIMS), I-CIMS, and TAG. Error bars represent instrumental error as described in section 2.5.

However, the average diurnal cycles of F_p show a similar temporal trend and magnitude between the instruments and the absorptive partitioning model, with higher F_p at night and lower during the day. The diurnal trend is more similar to the A-CIMS and I-CIMS (showing a slight offset) but is still close to the TAG diurnal cycle which increases later in the night than for the the CIMSs. The prediction of partitioning to the aqueous phase suggests a value of 0.05, so while it may contribute, the partitioning appears to be dominated by partitioning to the aerosol phase. Unlike pinonic acid, on average pinic acid

concentrations agree better for the particle phase data than the gas phase between the A-CIMS and TAG (see diurnal cycle), possibly due to the fact that there is more particle-phase signal for pinic acid and better S/N. The A-CIMS and TAG instruments show more diurnal variation in the particle and gas concentrations, while the I-CIMS change little throughout the day. Although not easily observable in the scatter plot, the gas phase diurnal cycles show an anti-correlation between the TAG and A-CIMS which also manifests itself in the total measurement (with somewhat lesser variation), with the A-CIMS measuring higher gas phase concentrations than the TAG, and peaking at night while the TAG peaks in the afternoon (while the I-CIMS stays fairly constant throughout the day). These complex differences might be due to some of the reasons discussed above, e.g. A-CIMS being more sensitive to an isomer of $C_9H_{14}O_4$ which is produced at during the day.

In Figure 6 the same additional A-CIMS and IMS-TOF information is shown for this elemental formula.

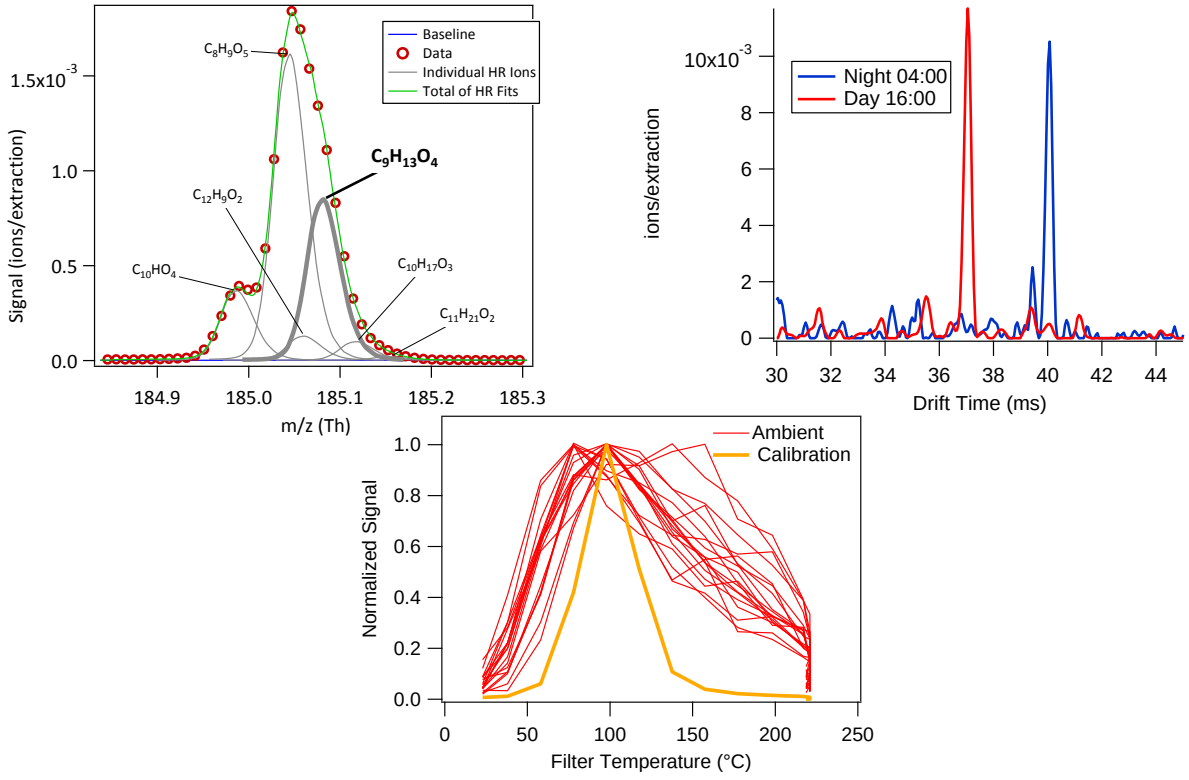

Figure 6. Extra information for the formula $C_9H_{14}O_4$ (pinic acid and isomers, measured in the A-CIMS as $C_9H_{13}O_4^-$). (A) High resolution signal fits averaged over one day. Formula under study is in bold. (B) Two one hour averaged ion mobility spectra, taken with an ion mobility nitrate chemical ionization mass spectrometer (C). Heating cycles from the A-CIMS, showing field data (red) vs temperature as the FIGAERO filter is slowly heated (see text for details). A calibration with a mixture is shown in yellow. See Figure 4 for more calibration details.

Figure 6a shows that this peak ($C_9H_{13}O_4^-$) is also a part of a larger group of peaks, adding some uncertainty to the quantification of its area. Figure 6b shows two averaged ion mobility spectra for the elemental formula $C_9H_{14}O_4$, during day and night. One of the isomers is present in the day and absent at night, and the other isomer is present at night and not during the day. Note that the IMS used nitrate chemical ionization and as such it may detect a different combination of isomers from the A-CIMS, I-CIMS and TAG. So while this cannot inform which isomers the A-CIMS detects, it does confirm that there are multiple isomers present and that they have variable relative concentrations during the day/night. In Figure 6c the ambient thermal desorption profiles show a range of peak desorption temperatures with the calibration compound approximately in the middle, in contrast to pinonic acid. The larger ambient width could be due to the presence of several isomers at this molecular formula that have slightly different volatilities (including thermal decomposition products). It could also be due to changing evaporation matrix effects.

3.1.4. Detailed Comparisons for Hydroxy Glutaric Acid

The comparison for $C_5H_8O_5$ ("hydroxy glutaric acid"), shown in Figure 7, shows similar issues to those of the other two examples.

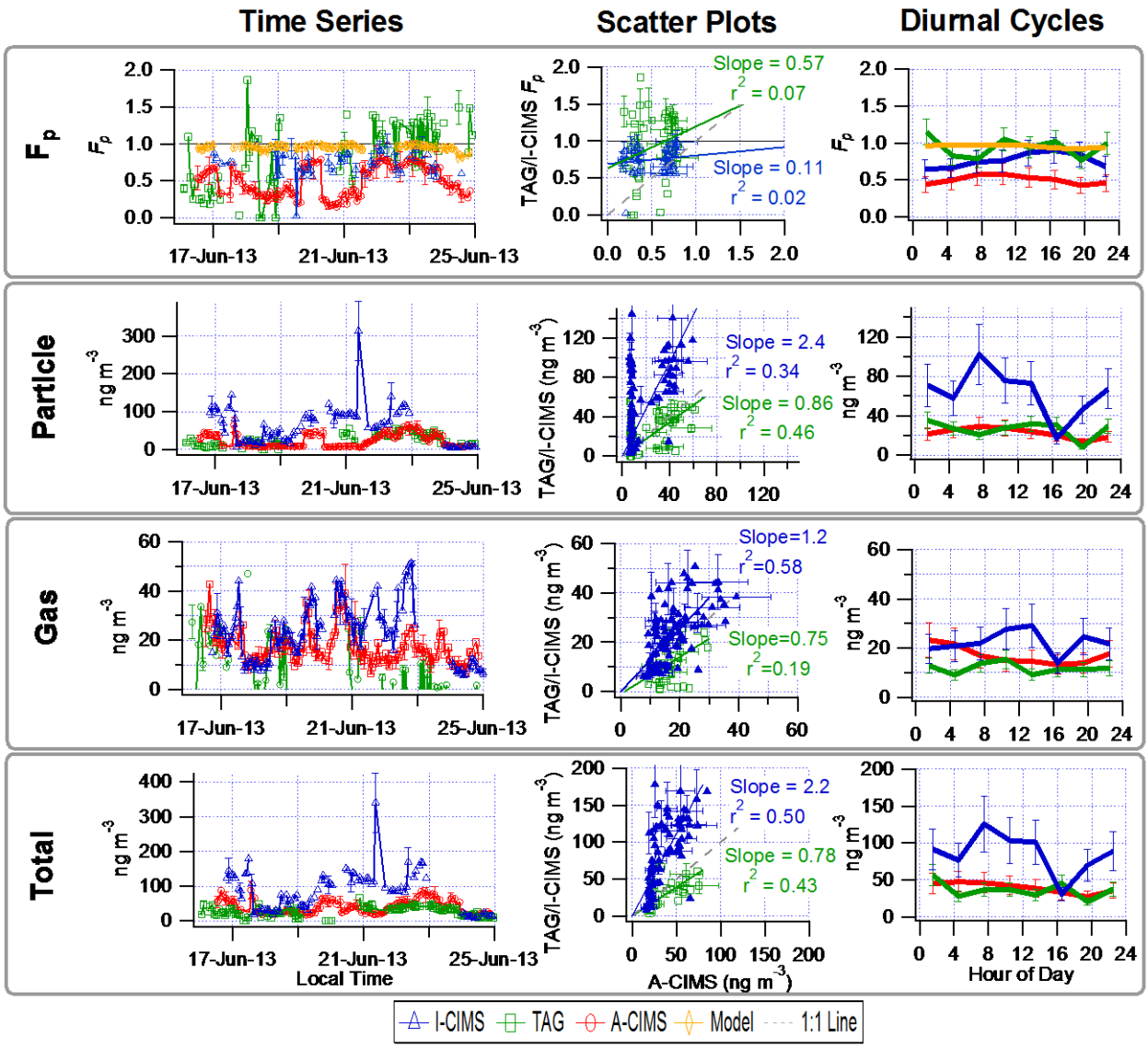

Figure 7. Time series (left), scatter plots (center) and diurnal cycles (right) of the measured gas/particle partitioning (F_p, top row), particle phase (2nd row), gas phase (3rd row) and total concentration (bottom row) for $C_5H_8O_5$ (hydroxy glutaric acid) the acetate (A-CIMS), I-CIMS, and TAG. Error bars represent instrumental error as described in section 2.5.

While there is a significant amount of scatter in F_p here, all instruments show two consistent results: 1) the diurnal cycles show a lack of variation over the course of the day, and 2) they all measure high particle partitioning values. The absorptive partitioning model predicts high partitioning values that do not vary throughout the day as well. The prediction of partitioning to the aqueous phase is 0.32. All the traces measure higher partitioning values than that so it again appears to be dominated by partitioning to

the aerosol phase. The gas phase shows more consistent concentrations among the three instruments, while the I-CIMS measures higher particle concentrations.

The high resolution mass spectral fitting for this elemental formula (Figure 8a) shows that $C_5H_7O_5^-$ is the main peak at *m/z* 147 for A-CIMS, making the peak-fitting uncertainty a relatively small source of error in the quantification.

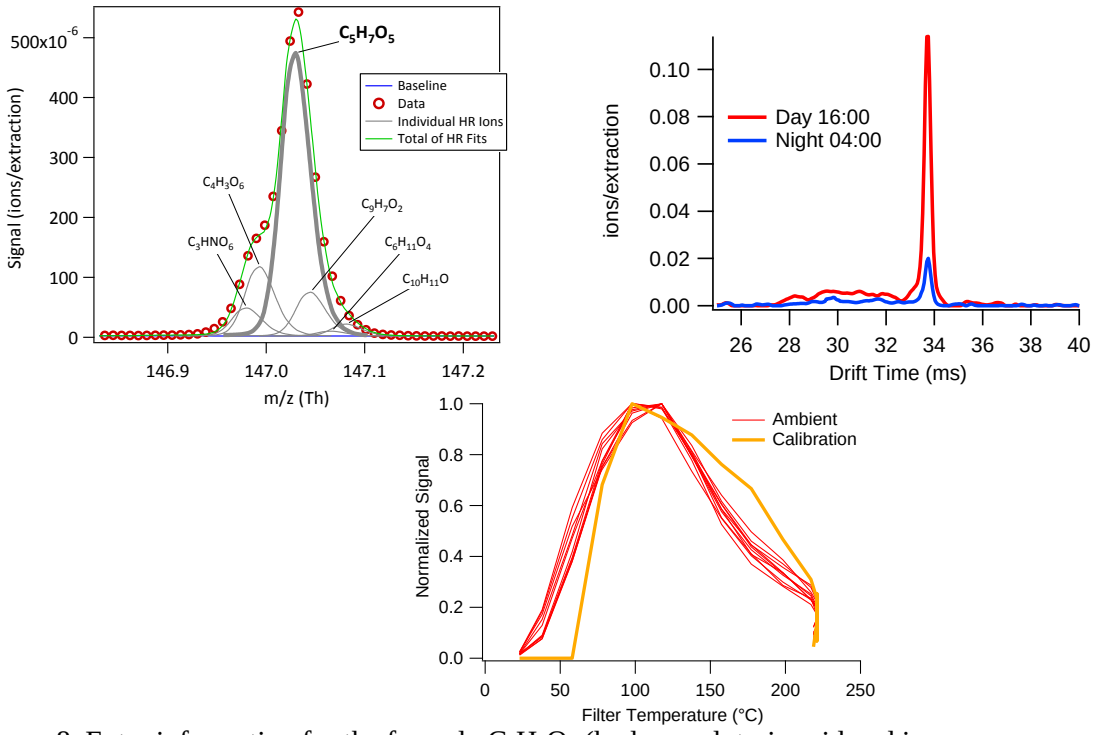

Figure 8. Extra information for the formula $C_5H_8O_5$ (hydroxy glutaric acid and isomers, measured in the A-CIMS as $C_5H_8O_4^-$). (A) HR fits from the A-CIMS. Formula being measured is in bold. (B) Two averaged ion mobility spectra, taken with an ion mobility nitrate chemical ionization mass spectrometer. (C) Heating cycles from the A-CIMS, showing field data (red) vs temperature as the FIGAERO filter is slowly heated (see text for details). A calibration with a mixture is shown in yellow. See Figure 4 for more calibration details.

The IMS spectra, shown in Figure 8b, show only one isomer at this elemental formula. All of the thermal desorption profiles, shown in Figure 8c, also closely match the calibration compound profile, suggesting that other isomers at different volatilities or the thermal decomposition of other compounds are not interfering with this signal for the A-CIMS. This still leaves the possibility that the compound itself is

partially thermally decomposing during the heating cycle and is therefore under-measured for the particle phase.

3.2. Comparison of A-CIMS and PTRMS

For the comparison between A-CIMS and PTRMS, 11 elemental formulas were chosen based on a match of the elemental formulas assigned to high-resolution peaks in the mass spectra. These are compounds for which there are very few possible isomers given their elemental formula (alkanoic acids; $C_XH_{2Y}O_2$).The compounds vary in their level of agreement. The comparison of the averaged F_p values for each of the commonly-measured elemental formulas is shown as a scatter plot in Figure 9a.

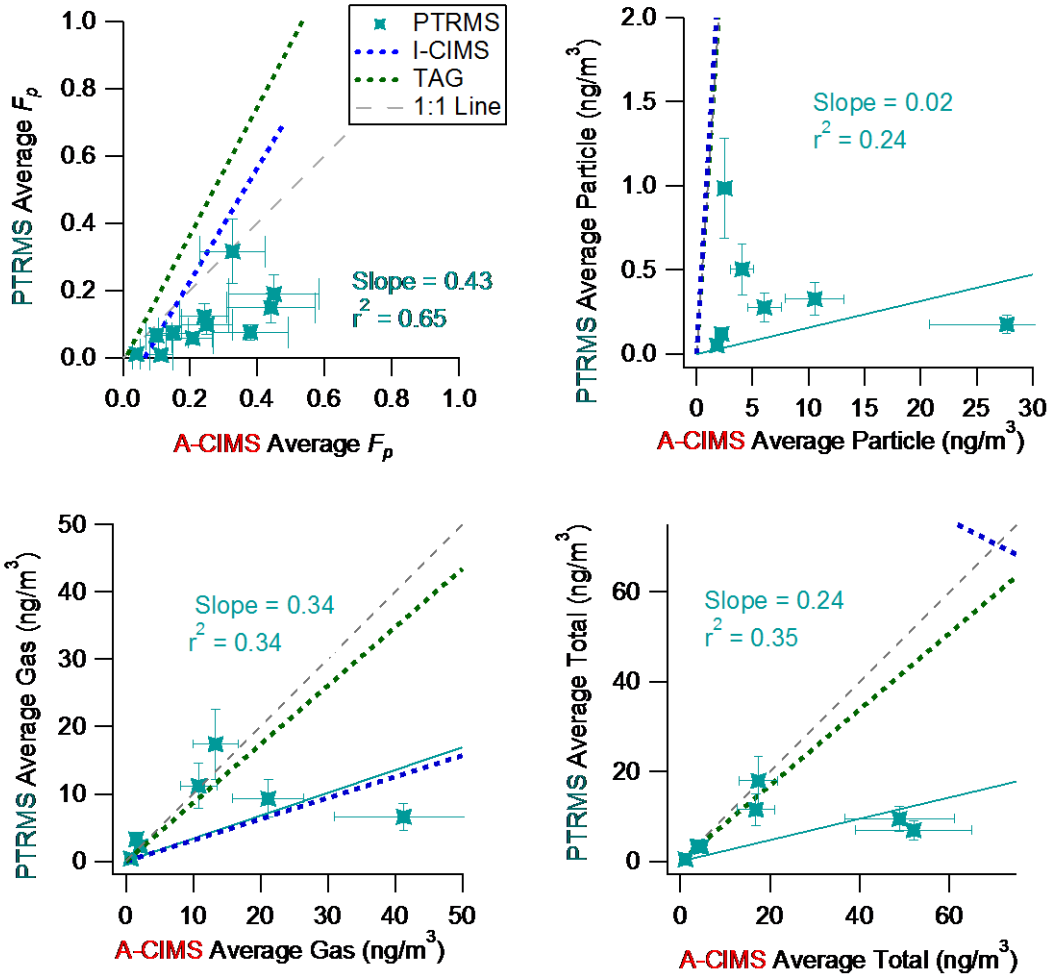

Figure 9. Scatter plot of the average measured F_p (a), particle concentration (b), gas concentration (c) and total concentration (d) over the entire overlap period from PTRMS vs. A-CIMS. Each points represents the average measurement for one compound. Lines of fit from the TAG and I-CIMS are shown in dotted lines for reference.

F_p measured by the PTRMS are, on average, about half of the F_p (slope = 0.43, r^2=0.65) vs. the A-CIMS. The largest discrepancy is the particle-phase concentrations (Fig. 9b), as the PTRMS consistently measures much lower values, while there is more similarity in the gas-phase and total measurements for several compounds (Fig. 9c-d). There are two possible reasons for this difference. First, the heated lines (200 °C) used in the PTRMS inlet system expose all compounds to those high temperatures and could cause some compounds to thermally decompose. Since both the gas and aerosol use the heated transfer lines that decomposition would affect them the same. By comparison, the A-CIMS only exposes the compounds to the temperature needed to evaporate them from the FIGAERO filter, and the bulk of the measured compounds in this study desorb in the range 70–120 ºC. Secondly, the two instruments could be measuring isomers with different functional groups, and thus different vapor pressures and partitioning values. Given that most of the compounds measured are alkanoic acids, there are only a few other possible isomers. One is a hydroxycarbonyl instead of a carboxylic acid group, but according to structure-activity relationships (Pankow and Asher, 2008) that would not change the estimated vapor pressure of the molecule by a substantial amount.

An example time series of F_p along with gas and particle phase concentrations can be found in Figure 10 for “heptadecanoic acid.”

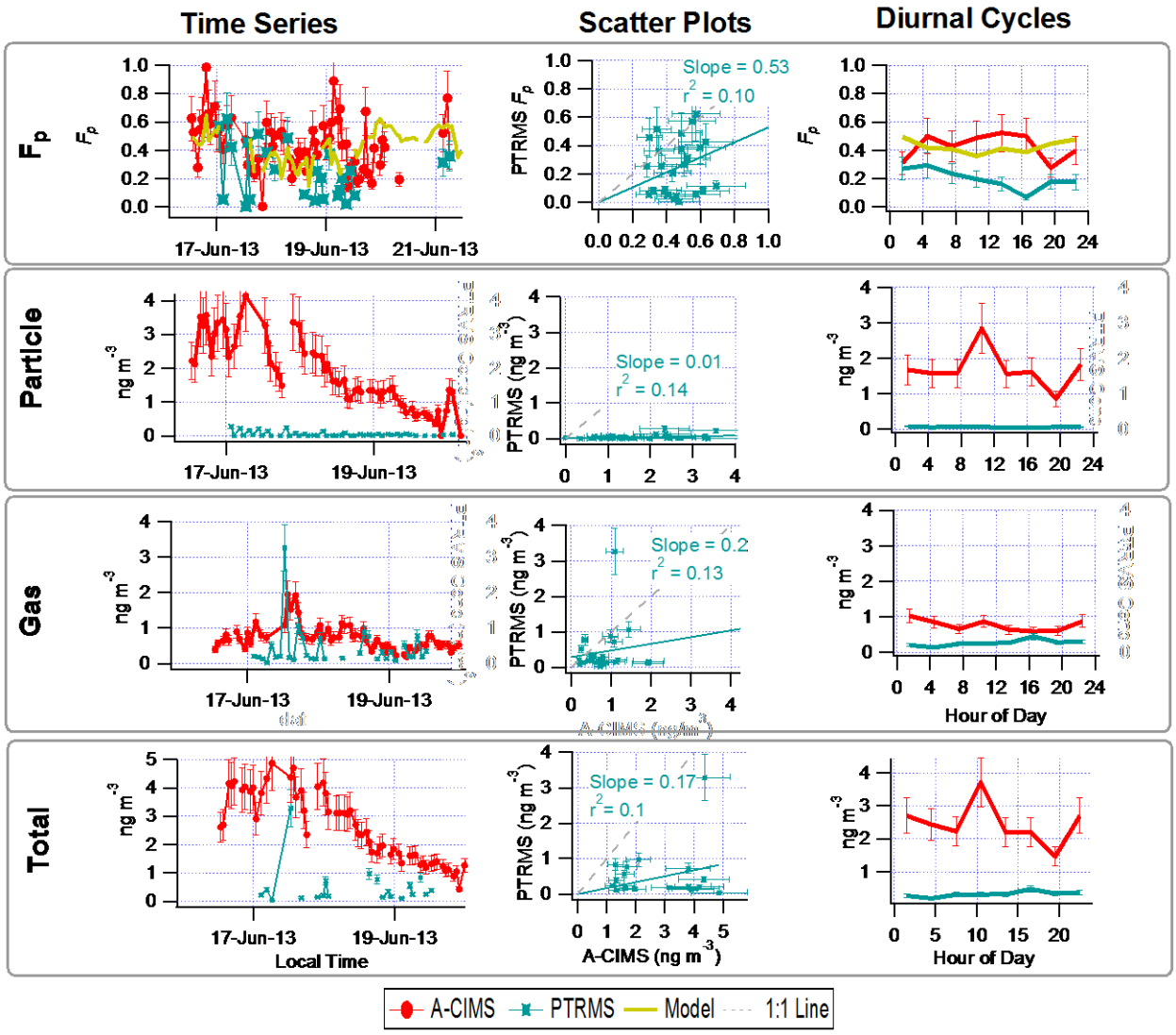

Figure 10. Time series (left), scatter plot (center) and diurnal cycle (right) of the measured gas/particle partitioning (F_p), particle phase, gas phase, and total concentration for $C_{17}H_{34}O_2$ (heptadecanoic acid) the acetate (A-CIMS) and PTRMS. *C** used for the model here is from Nannoolal et al. (2008)

The partitioning values do not agree in either magnitude or temporal trends, with the A-CIMS being closer to the model values (see diurnal cycles of F_p). As discussed above for the average data for all compounds, the largest difference in concentration is observed for the particle phase, which is much lower in the PTRMS than in the A-CIMS. The gas phase concentrations are more similar, although neither are well correlated. Figure 11 shows the thermal desorption profiles for the A-CIMS and the PTRMS along with a calibration done with the A-CIMS instrument.

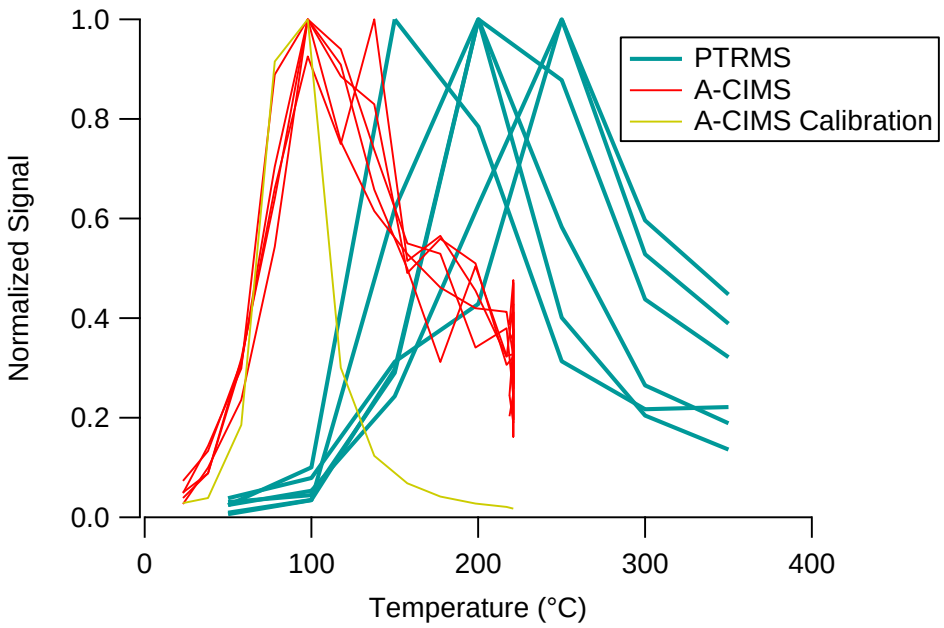

Figure 11. Heating cycles from the A-CIMS, showing field data (red) vs filter temperature as the FIGAERO filter is slowly heated (see text for details). A calibration with a mixture done with the A-CIMS is shown in yellow. PTRMS signal vs temperature as the CTD cell is heated is shown in blue (no calibration available).

In the A-CIMS the profiles are very consistent and the peak desorption temperature is similar to the calibration compound, with the possibility of some interference at higher temperatures. The PTRMS shows much higher peak desorption temperatures, which vary from run to run. There is no calibration data to compare to for this instrument, but similar compounds tested in previous work suggest that a compound of this volatility desorbed around 150ºC. (Holzinger et al., 2010a)

4. **Conclusions**

We have presented the first intercomparison of in-situ near real-time measurements of gas/particle partitioning, a very recently developed capability. We use measurements from the SOAS field campaign in the southeastern US in the summer of 2013. Although the individual time series of partitioning fractions show a substantial amount of scatter, the three acids compared between the A-CIMS, I-CIMS and the TAG span the range of possible F_p values and show better agreement when averaged into campaign-long averages. They also follow the trend of model values with species volatility. The fourth

instrument, the PTRMS, showed overall lower aerosol partitioning values than the A-CIMS, less than half, and most of the difference appears to result from the particle phase measurements.

Discrepancies could, in part, be attributed to measuring multiple/different isomers of the same elemental formula being measured by the different instruments. The ion mobility spectrum shows that multiple isomers were present at one of the elemental formulas discussed in this paper, and the thermal desorption profiles suggest that there could be multiple isomers present in the particle phase in some cases. Thermal decomposition of the molecules of interest in the inlet lines and inside instruments may also have contributed to scatter in the partitioning values. Another likely cause for discrepancies is the thermal decomposition of larger molecules (oligomers) into smaller molecules (monomers) detected as the molecules of interest. Thermal desorption profiles from the A-CIMS shows that thermal decomposition of larger oligomers into the compound of interest may be happening in some cases. Discrepancies may also be due to inlet losses or other unidentified adsorption/inlet issues.

It is worth noting that the TAG instrument has already been re-deployed with lower noise and estimated uncertainties, and the FIGAERO inlet used on the A-CIMS and I-CIMS has been improved since this data was collected. This was the first field campaign where these instruments were together, and shows the need for a more thorough instrument comparisons in the laboratory. It also shows the importance and value of using all available data when using CIMS measurements (e.g., HR fits, thermograms). Finally, there is a pressing need for separation techniques (such as the IMS-TOF) that can be interfaced to the CIMS instruments to allow better separation of structural isomers.

Bibliography

Alley, R., Berntsen, T., Bindoff, N. L., Chen, Z., Chidthaisong, A., Friedlingstein, P., Hegerl, G., Heimann, M., Hewitson, B., Hoskins, B., Joos, F., Jouzel, J., Kattsov, V., Lohmann, U., Manning, M., Matsuno, T., Molina, M., Nicholls, N., Overpeck, J., Qin, D., Ramaswamy, V., Ren, J., Rusticucci, M., Solomon, S., Somerville, R., Stocker, T. F., Stott, P., Stouffer, R. J., Whetton, P., Wood, R. A., Wratt, D., Arblaster, J., Brasseur, G., Christensen, J. H., Denman, K., Fahey, D. W., Forster, P., Jansen, E., Jones, P. D., Knutti, R., Treut, H. Le, Lemke, P., Meehl, G., Mote, P., Randall, D., Stone, D. A., Trenberth, E., Willebrand, J. and Zwiers, F.: INTERGOVERNMENTAL PANEL ON CLIMATE CHANGE Climate Change 2007 : The Physical Science Basis Summary for Policymakers Contribution of Working Group I to the Fourth Assessment Report of the Intergovernmental Panel on Climate Change, 2007.

Andrews, D. U., Heazlewood, B. R., Maccarone, A. T., Conroy, T., Payne, R. J., Jordan, M. J. T. and Kable, S. H.: Photo-tautomerization of acetaldehyde to vinyl alcohol: a potential route to tropospheric acids., Science, 337(6099), 1203–6, doi:10.1126/science.1220712, 2012.

Bilde, M., Barsanti, K., Booth, M., Cappa, C. D., Donahue, N. M., Emanuelsson, E. U., McFiggans, G., Krieger, U. K., Marcolli, C., Topping, D., Ziemann, P., Barley, M., Clegg, S., Dennis-Smither, B., Hallquist, M., Hallquist, Å. M., Khlystov, A., Kulmala, M., Mogensen, D., Percival, C. J., Pope, F., Reid, J. P., Ribeiro da Silva, M. a. V., Rosenoern, T., Salo, K., Soonsin, V. P., Yli-Juuti, T., Prisle, N. L., Pagels, J., Rarey, J., Zardini, A. a. and Riipinen, I.: Saturation Vapor Pressures and Transition Enthalpies of Low-Volatility Organic Molecules of Atmospheric Relevance: From Dicarboxylic Acids to Complex Mixtures, Chem. Rev., 150501082359009, doi:10.1021/cr5005502, 2015.

Bilde, M. and Pandis, S. N.: Evaporation Rates and Vapor Pressures of Individual Aerosol Species Formed in the Atmospheric Oxidation of α- and β-Pinene, Environ. Sci. Technol., 35(16), 3344–3349, doi:10.1021/es001946b, 2001.

Chebbi, A. and Carlier, P.: Carboxylic acids in the troposphere, occurrence, sources, and sinks: A review, Atmos. Environ., 30(24), 4233–4249, doi:10.1016/1352-2310(96)00102-1, 1996.

Compernolle, S. and Müller, J.-F.: Henry's law constants of diacids and hydroxypolyacids: recommended values, Atmos. Chem. Phys., 13(9), 25125–25156, doi:10.5194/acpd-13-25125-2013, 2013.

Decarlo, P. F., Kimmel, J. R., Trimborn, A., Northway, M. J., Jayne, J. T., Aiken, A. C., Gonin, M., Fuhrer, K., Horvath, T., Docherty, K. S., Worsnop, D. R. and Jimenez, J. L.: Field-Deployable, High-Resolution, Time-of-Flight Aerosol Mass Spectrometer, Anal. Chem., 78(24), 8281–8289, doi:8410.1029/2001JD001213.Analytical, 2006.

Donahue, N. M., Robinson, A. L., Stanier, C. O. and Pandis, S. N.: Coupled partitioning, dilution, and chemical aging of semivolatile organics., Environ. Sci. Technol., 40(8), 2635–43 [online] Available from: http://www.ncbi.nlm.nih.gov/pubmed/16683603 (Accessed 21 January 2014), 2006.

Dzepina, K., Volkamer, R. M., Madronich, S., Tulet, P., Ulbrich, I. M., Zhang, Q., Cappa, C. D., Ziemann, P. J. and Jimenez, J. L.: Evaluation of recently-proposed secondary organic aerosol models for a case study in Mexico City, Atmos. Chem. Phys., 9(15), 5681–5709, doi:10.5194/acp-9-5681-2009,

2009.

Eiceman, G. A. and Karpas, Z.: Ion Mobility Spectrometry, Second Edition, Taylor & Francis., 2010.

Ervens, B.: Modeling the Processing of Aerosol and Trace Gases in Clouds and Fogs., Chem. Rev., doi:10.1021/cr5005887, 2015.

F.D. Lopez-Hilfiker, C. Mohr, E.L. D'Ambro, A. Lutz, T.P. Riedel, C.J. Gaston, S. Iyer, Z. Zhang, A. Gold, J.D. Surratt, B.H. Lee, T. Kurten, W.W. Hu, J.L. Jimenez, M. Hallquist, J. A. T.: Molecular composition and volatility of organic aerosol formed in a polluted isoprene-rich region, Submitt. to Environ. Sci. Technol., 2015.

Goldstein, A. H. and Galbally, I. E.: Known and unexplored organic constituents in the earth's atmosphere, Environ. Sci. Technol., 41(5), 1515–1521 [online] Available from: http://pubs.acs.org/doi/abs/10.1021/es072476p (Accessed 26 December 2013), 2007.

de Gouw, J. a.: Budget of organic carbon in a polluted atmosphere: Results from the New England Air Quality Study in 2002, J. Geophys. Res., 110(D16), D16305, doi:10.1029/2004JD005623, 2005.

De Gouw, J. and Jimenez, J. L.: Organic Aerosols in the Earth's Atmosphere, Environ. Sci. Technol., 43(20), 7614–7618, doi:Doi 10.1021/Es9006004, 2009.

Hallquist, M., Wenger, J. C., Baltensperger, U., Rudich, Y., Simpson, D., Claeys, M., Dommen, J., Donahue, N. M., George, C., Goldstein, A. H., Hamilton, J. F., Herrmann, H., Hoffmann, T., Iinuma, Y., Jang, M., Jenkin, M. E., Jimenez, J. L., Kiendler-Scharr, A., Maenhaut, W., McFiggans, G., Mentel, T. F., Monod, A., Prévôt, A. S. H., Seinfeld, J. H., Surratt, J. D., Szmigielski, R. and Wildt, J.: The formation, properties and impact of secondary organic aerosol: current and emerging issues, Atmos. Chem. Phys., 9(14), 5155–5236, doi:10.5194/acp-9-5155-2009, 2009.

Harald Stark, Reddy L.N. Yatavelli, Samantha L. Thompson, Joel R. Kimmel, Michael J. Cubison, Puneet S. Chhabra, Manjula R. Canagaratna, John T. Jayne, Douglas R. Worsnop, J. L. J.: Methods to extract molecular and bulk chemical information from series of complex mass spectra with limited mass resolution, Int. J. Mass Spectrom., 389, 26–38, 2015.

Holzinger, R., Kasper-Giebl, A., Staudinger, M., Schauer, G. and Röckmann, T.: Analysis of the chemical composition of organic aerosol at the Mt. Sonnblick observatory using a novel high mass resolution thermal-desorption proton-transfer-reaction mass-spectrometer (hr-TD-PTR-MS), Atmos. Chem. Phys., 10(20), 10111–10128, doi:10.5194/acp-10-10111-2010, 2010a.

Holzinger, R., Williams, J., Herrmann, F., Lelieveld, J., Donahue, N. M. and Röckmann, T.: Aerosol analysis using a Thermal-Desorption Proton-Transfer-Reaction Mass Spectrometer (TD-PTR-MS): a new approach to study processing of organic aerosols, Atmos. Chem. Phys., 10(5), 2257–2267, doi:10.5194/acp-10-2257-2010, 2010b.

Hu, W. W., Campuzano-Jost, P., Palm, B. B., Day, D. A., Ortega, A. M., Hayes, P. L., Krechmer, J. E., Chen, Q., Kuwata, M., Liu, Y. J., de Sá, S. S., Martin, S. T., Hu, M., Budisulistiorini, S. H., Riva, M., Surratt, J. D., St. Clair, J. M., Isaacman-Van Wertz, G., Yee, L. D., Goldstein, A. H., Carbone, S., Artaxo, P., de Gouw, J. A., Koss, A., Wisthaler, A., Mikoviny, T., Karl, T., Kaser, L., Jud, W., Hansel, A.,

Docherty, K. S., Robinson, N. H., Coe, H., Allan, J. D., Canagaratna, M. R., Paulot, F., Jimenez, J. L., McKinney, K., Martin, S. T., Hu, M., Budisulistiorini, S. H., Riva, M., Surratt, J. D., St. Clair, J. M., Isaacman-Van Wertz, G., Yee, L. D., Goldstein, A. H., Carbone, S., Brito, J., Artaxo, P., de Gouw, J. A., Koss, A., Wisthaler, A., Mikoviny, T., Karl, T., Kaser, L., Jud, W., Hansel, A., Docherty, K. S., Alexander, M. L., Robinson, N. H., Coe, H., Allan, J. D., Canagaratna, M. R., Paulot, F. and Jimenez, J. L.: Characterization of a real-time tracer for Isoprene Epoxydiols-derived Secondary Organic Aerosol (IEPOX-SOA) from aerosol mass spectrometer measurements, Atmos. Chem. Phys., 15(8), 11223–11276, doi:10.5194/acpd-15-11223-2015, 2015.

Isaacman, G., Kreisberg, N. M., Yee, L. D., Worton, D. R., Chan, A. W. H., Moss, J. A., Hering, S. V. and Goldstein, A. H.: Online derivatization for hourly measurements of gas- and particle-phase semi-volatile oxygenated organic compounds by thermal desorption aerosol gas chromatography (SV-TAG), Atmos. Meas. Tech., 7(12), 4417–4429, doi:10.5194/amt-7-4417-2014, 2014.

Jimenez, J. L., Canagaratna, M. R., Donahue, N. M., Prevot, a S. H., Zhang, Q., Kroll, J. H., DeCarlo, P. F., Allan, J. D., Coe, H., Ng, N. L., Aiken, a C., Docherty, K. S., Ulbrich, I. M., Grieshop, a P., Robinson, a L., Duplissy, J., Smith, J. D., Wilson, K. R., Lanz, V. a, Hueglin, C., Sun, Y. L., Tian, J., Laaksonen, a, Raatikainen, T., Rautiainen, J., Vaattovaara, P., Ehn, M., Kulmala, M., Tomlinson, J. M., Collins, D. R., Cubison, M. J., Dunlea, E. J., Huffman, J. a, Onasch, T. B., Alfarra, M. R., Williams, P. I., Bower, K., Kondo, Y., Schneider, J., Drewnick, F., Borrmann, S., Weimer, S., Demerjian, K., Salcedo, D., Cottrell, L., Griffin, R., Takami, a, Miyoshi, T., Hatakeyama, S., Shimono, a, Sun, J. Y., Zhang, Y. M., Dzepina, K., Kimmel, J. R., Sueper, D., Jayne, J. T., Herndon, S. C., Trimborn, a M., Williams, L. R., Wood, E. C., Middlebrook, a M., Kolb, C. E., Baltensperger, U. and Worsnop, D. R.: Evolution of organic aerosols in the atmosphere., Science, 326(5959), 1525–9, doi:10.1126/science.1180353, 2009.

Kanakidou, M., Seinfeld, J. H., Pandis, S. N., Barnes, I., Dentener, F. J., Facchini, M. C., Van Dingenen, R., Ervens, B., Nenes, A., Nielsen, C. J., Swietlicki, E., Putaud, J. P., Balkanski, Y., Fuzzi, S., Horth, J., Moortgat, G. K., Winterhalter, R., Myhre, C. E. L., Tsigaridis, K., Vignati, E., Stephanou, E. G. and Wilson, J.: Organic aerosol and global climate modelling: a review, Atmos. Chem. Phys., 5(4), 1053–1123, doi:10.5194/acp-5-1053-2005, 2005.

Kaplan, K., Graf, S., Tanner, C., Gonin, M., Fuhrer, K., Knochenmuss, R., Dwivedi, P. and Hill, H. H.: Resistive glass IM-TOFMS., Anal. Chem., 82(22), 9336–43, doi:10.1021/ac1017259, 2010.

Lee, B. H., Lopez-Hilfiker, F. D., Mohr, C., Kurtén, T., Worsnop, D. R. and Thornton, J. A.: An Iodide-Adduct High-Resolution Time-of-Flight Chemical-Ionization Mass Spectrometer: Application to Atmospheric Inorganic and Organic Compounds., Environ. Sci. Technol., 48(11), 6309–17, doi:10.1021/es500362a, 2014.

Lim, Y. B., Tan, Y., Perri, M. J., Seitzinger, S. P. and Turpin, B. J.: Aqueous chemistry and its role in secondary organic aerosol (SOA) formation, Atmos. Chem. Phys., 10(21), 10521–10539, doi:10.5194/acp-10-10521-2010, 2010.

Lopez-Hilfiker, F. D., Mohr, C., Ehn, M., Rubach, F., Kleist, E., Wildt, J., Mentel, T. F., Carrasquillo, A. J., Daumit, K. E., Hunter, J. F., Kroll, J. H., Worsnop, D. R. and Thornton, J. A.: Phase partitioning and volatility of secondary organic aerosol components formed from α-pinene ozonolysis and OH oxidation:

the importance of accretion products and other low volatility compounds, Atmos. Chem. Phys., 15(4), 7765–7776, doi:10.5194/acp-15-7765-2015, 2015.

Lopez-Hilfiker, F. D., Mohr, C., Ehn, M., Rubach, F., Kleist, E., Wildt, J., Mentel, T. F., Lutz, A., Hallquist, M., Worsnop, D. and Thornton, J. A.: A novel method for on-line analysis of gas and particle composition: description and evaluation of a Filter Inlet for Gases and AEROsols (FIGAERO), Atmos. Meas. Tech., 6(4), 9347–9395, doi:10.5194/amt-7-983-2014, 2013.

Mahowald, N.: Aerosol indirect effect on biogeochemical cycles and climate., Science, 334(6057), 794–6, doi:10.1126/science.1207374, 2011.

Müller, L., Reinnig, M.-C., Naumann, K. H., Saathoff, H., Mentel, T. F., Donahue, N. M. and Hoffmann, T.: Formation of 3-methyl-1,2,3-butanetricarboxylic acid via gas phase oxidation of pinonic acid – a mass spectrometric study of SOA aging, Atmos. Chem. Phys., 12(3), 1483–1496, doi:10.5194/acp-12-1483-2012, 2012.

Nannoolal, Y., Rarey, J. and Ramjugernath, D.: Estimation of pure component properties, Fluid Phase Equilib., 269(1-2), 117–133, doi:10.1016/j.fluid.2008.04.020, 2008.

Nguyen, T. K. V., Petters, M. D., Suda, S. R., Guo, H., Weber, R. J. and Carlton, a. G.: Trends in particle-phase liquid water during the Southern Oxidant and Aerosol Study, Atmos. Chem. Phys., 14(20), 10911–10930, doi:10.5194/acp-14-10911-2014, 2014.

O'Brien, R. E., Neu, A., Epstein, S. A., Macmillan, A. C., Wang, B., Kelly, S. T., Nizkorodov, S. A., Laskin, A., Moffet, R. C. and Gilles, M. K.: Physical properties of ambient and laboratory-generated secondary organic aerosol, Geophys. Res. Lett., 4347–4353, doi:10.1002/2014GL060219.Received, 2014.

Odum, J. R., Hoffmann, T., Bowman, F., Collins, D., Flagan Richard, C., Seinfeld John, H., Flagan, R. C. and Seinfeld, J. H.: Gas particle partitioning and secondary organic aerosol yields, Environ. Sci. Technol., 30(8), 2580–2585, doi:10.1021/es950943+, 1996.

Pankow, J. F.: An absorption model of gas/particle partitioning of organic compounds in the atmosphere, Atmos. Environ., 28(2), 185–188, doi:10.1016/1352-2310(94)90093-0, 1994.

Pankow, J. F. and Asher, W. E.: SIMPOL.1: a simple group contribution method for predicting vapor pressures and enthalpies of vaporization of multifunctional organic compounds, Atmos. Chem. Phys., 8(10), 2773–2796, doi:10.5194/acp-8-2773-2008, 2008.

Perraud, V., Bruns, E. a, Ezell, M. J., Johnson, S. N., Yu, Y., Alexander, M. L., Zelenyuk, A., Imre, D., Chang, W. L., Dabdub, D., Pankow, J. F. and Finlayson-Pitts, B. J.: Nonequilibrium atmospheric secondary organic aerosol formation and growth., Proc. Natl. Acad. Sci. U. S. A., 109(8), 2836–41, doi:10.1073/pnas.1119909109, 2012.

Pope, C. A., Ezzati, M. and Dockery, D. W.: Fine-particulate air pollution and life expectancy in the United States., N. Engl. J. Med., 360(4), 376–86, doi:10.1056/NEJMsa0805646, 2009.

Price, H. C., Murray, B. J., Mattsson, J., O'Sullivan, D., Wilson, T. W., Baustian, K. J. and Benning, L. G.: Quantifying water diffusion in high-viscosity and glassy aqueous solutions using a Raman isotope tracer method, Atmos. Chem. Phys., 13(8), 3817–3830, doi:10.5194/acpd-13-29375-2013, 2013.

Renbaum-Wolff, L., Grayson, J. W., Bateman, A. P., Kuwata, M., Sellier, M., Murray, B. J., Shilling, J. E., Martin, S. T. and Bertram, A. K.: Viscosity of α-pinene secondary organic material and implications for particle growth and reactivity., Proc. Natl. Acad. Sci. U. S. A., 110(20), 8014–9, doi:10.1073/pnas.1219548110, 2013.

Rollins, A. W., Pusede, S., Wooldridge, P., Min, K.-E., Gentner, D. R., Goldstein, A. H., Liu, S., Day, D. A., Russell, L. M., Rubitschun, C. L., Surratt, J. D. and Cohen, R. C.: Gas/particle partitioning of total alkyl nitrates observed with TD-LIF in Bakersfield, J. Geophys. Res. Atmos., 118(12), 6651–6662, doi:10.1002/jgrd.50522, 2013.

Saleh, R., Donahue, N. M. and Robinson, A. L.: Time Scales for Gas-Particle Partitioning Equilibration of Secondary Organic Aerosol Formed from Alpha-Pinene Ozonolysis., Environ. Sci. Technol., doi:10.1021/es400078d, 2013.

Shiraiwa, M., Ammann, M., Koop, T. and Poschl, U.: Gas uptake and chemical aging of semisolid organic aerosol particles, Proc. Natl. Acad. Sci. U. S. A., 108(27), 11003–11008, doi:DOI 10.1073/pnas.1103045108, 2011.

Szmigielski, R., Surratt, J. D., Gómez-González, Y., Veken, P. Van der, Kourtchev, I., Vermeylen, R., Blockhuys, F., Jaoui, M., Kleindienst, T. E., Lewandowski, M., Offenberg, J. H., Edney, E. O., Seinfeld, J. H., Maenhaut, W. and Claeys, M.: 3-methyl-1,2,3-butanetricarboxylic acid: An atmospheric tracer for terpene secondary organic aerosol, Geophys. Res. Lett., 34(24), 2007.

Tsigaridis, K., Daskalakis, N., Kanakidou, M., Adams, P. J., Artaxo, P., Bahadur, R., Balkanski, Y., Bauer, S. E., Bellouin, N., Benedetti, A., Bergman, T., Berntsen, T. K., Beukes, J. P., Bian, H., Carslaw, K. S., Chin, M., Curci, G., Diehl, T., Easter, R. C., Ghan, S. J., Gong, S. L., Hodzic, A., Hoyle, C. R., Iversen, T., Jathar, S., Jimenez, J. L., Kaiser, J. W., Kirkevåg, A., Koch, D., Kokkola, H., Lee, Y. H., Lin, G., Liu, X., Luo, G., Ma, X., Mann, G. W., Mihalopoulos, N., Morcrette, J.-J., Müller, J.-F., Myhre, G., Myriokefalitakis, S., Ng, S., O'Donnell, D., Penner, J. E., Pozzoli, L., Pringle, K. J., Russell, L. M., Schulz, M., Sciare, J., Seland, Ø., Shindell, D. T., Sillman, S., Skeie, R. B., Spracklen, D., Stavrakou, T., Steenrod, S. D., Takemura, T., Tiitta, P., Tilmes, S., Tost, H., van Noije, T., van Zyl, P. G., von Salzen, K., Yu, F., Wang, Z., Zaveri, R. a., Zhang, H., Zhang, K., Zhang, Q., Zhang, X. and Ng, N. L.: The AeroCom evaluation and intercomparison of organic aerosol in global models, Atmos. Chem. Phys., 14(5), 6027–6161, doi:10.5194/acpd-14-6027-2014, 2014.

Upshur, M. A., Strick, B. F., McNeill, V. F., Thomson, R. J. and Geiger, F. M.: Climate-relevant physical properties of molecular constituents for isoprene-derived secondary organic aerosol material, Atmos. Chem. Phys., 14(19), 10731–10740, doi:10.5194/acp-14-10731-2014, 2014.

Vaden, T. D., Imre, D., Beránek, J., Shrivastava, M. and Zelenyuk, A.: Evaporation kinetics and phase of laboratory and ambient secondary organic aerosol., Proc. Natl. Acad. Sci. U. S. A., 108(6), 2190–5, doi:10.1073/pnas.1013391108, 2011.

Vaden, T. D., Song, C., Zaveri, R. A., Imre, D. and Zelenyuk, A.: Morphology of mixed primary and secondary organic particles and the adsorption of spectator organic gases during aerosol formation., Proc. Natl. Acad. Sci. U. S. A., 107(15), 6658–63, doi:10.1073/pnas.0911206107, 2010.

Veres, P. R., Roberts, J. M., Cochran, A. K., Gilman, J. B., Kuster, W. C., Holloway, J. S., Graus, M., Flynn, J., Lefer, B., Warneke, C. and de Gouw, J.: Evidence of rapid production of organic acids in an urban air mass, Geophys. Res. Lett., 38(17), n/a–n/a, doi:10.1029/2011GL048420, 2011.

Veres, P., Roberts, J. M., Warneke, C., Welsh-Bon, D., Zahniser, M., Herndon, S., Fall, R. and de Gouw, J.: Development of negative-ion proton-transfer chemical-ionization mass spectrometry (NI-PT-CIMS) for the measurement of gas-phase organic acids in the atmosphere, Int. J. Mass Spectrom., 274(1-3), 48–55, doi:10.1016/j.ijms.2008.04.032, 2008.

Virtanen, A., Joutsensaari, J., Koop, T., Kannosto, J., Yli-Pirilä, P., Leskinen, J., Mäkelä, J. M., Holopainen, J. K., Pöschl, U., Kulmala, M., Worsnop, D. R. and Laaksonen, A.: An amorphous solid state of biogenic secondary organic aerosol particles., Nature, 467(7317), 824–7, doi:10.1038/nature09455, 2010.

Vogel, A. L., Äijälä, M., Brüggemann, M., Ehn, M., Junninen, H., Petäjä, T., Worsnop, D. R., Kulmala, M., Williams, J. and Hoffmann, T.: Online atmospheric pressure chemical ionization ion trap mass spectrometry (APCI-IT-MS^n) for measuring organic acids in concentrated bulk aerosol – a laboratory and field study, Atmos. Meas. Tech., 6(2), 431–443, doi:10.5194/amt-6-431-2013, 2013.

Volkamer, R., Jimenez, J. L., San Martini, F., Dzepina, K., Zhang, Q., Salcedo, D., Molina, L. T., Worsnop, D. R. and Molina, M. J.: Secondary organic aerosol formation from anthropogenic air pollution: Rapid and higher than expected, Geophys. Res. Lett., 33(17), L17811, doi:10.1029/2006GL026899, 2006.

Watson, J. G.: Visibility: science and regulation., J. Air Waste Manag. Assoc., 52(6), 628–713 [online] Available from: http://www.ncbi.nlm.nih.gov/pubmed/12074426 (Accessed 18 May 2015), 2002.

Yatavelli, R. L. N., Lopez-Hilfiker, F., Wargo, J. D., Kimmel, J. R., Cubison, M. J., Bertram, T. H., Jimenez, J. L., Gonin, M., Worsnop, D. R. and Thornton, J. a.: A Chemical Ionization High-Resolution Time-of-Flight Mass Spectrometer Coupled to a Micro Orifice Volatilization Impactor (MOVI-HRToF-CIMS) for Analysis of Gas and Particle-Phase Organic Species, Aerosol Sci. Technol., 46(12), 1313–1327, doi:10.1080/02786826.2012.712236, 2012.

Yatavelli, R. L. N., Mohr, C., Stark, H., Day, D. A., Thompson, S. L., Lopez-Hilfiker, F. D., Campuzano-Jost, P., Palm, B. B., Vogel, A. L., Hoffmann, T., Heikkinen, L., Äijälä, M., Ng, N. L., Kimmel, J. R., Canagaratna, M. R., Ehn, M., Junninen, H., Cubison, M. J., Petäjä, T., Kulmala, M., Jayne, J. T., Worsnop, D. R. and Jimenez, J. L.: Estimating the contribution of organic acids to northern hemispheric continental organic aerosol, Geophys. Res. Lett., 42(14), n/a–n/a, doi:10.1002/2015GL064650, 2015.

Yatavelli, R. L. N., Stark, H., Thompson, S. L., Kimmel, J. R., Cubison, M. J., Day, D. A., Campuzano-Jost, P., Palm, B. B., Hodzic, A., Thornton, J. A., Jayne, J. T., Worsnop, D. R. and Jimenez, J. L.: Semicontinuous measurements of gas–particle partitioning of organic acids in a ponderosa pine forest using a MOVI-HRToF-CIMS, Atmos. Chem. Phys., 14(3), 1527–1546, doi:10.5194/acp-14-1527-2014, 2014.

Yatavelli, R. L. N. and Thornton, J. a.: Particulate Organic Matter Detection Using a Micro-Orifice Volatilization Impactor Coupled to a Chemical Ionization Mass Spectrometer (MOVI-CIMS), Aerosol

Sci. Technol., 44(1), 61–74, doi:10.1080/02786820903380233, 2010.

Yong Jie Li, Pengfei Liu, Zhaoheng Gong, Yan Wang, Adam P. Bateman, Clara Bergoend, Allan K. Bertram, S. T. M.: Chemical Reactivity and Liquid/Nonliquid States of Secondary Organic Material, Enviromental Sci. Technol., doi:10.1021/acs.est.5b03392, 2015.

Zhang, Q., Jimenez, J. L., Canagaratna, M. R., Allan, J. D., Coe, H., Ulbrich, I., Alfarra, M. R., Takami, A., Middlebrook, A. M., Sun, Y. L., Dzepina, K., Dunlea, E., Docherty, K., DeCarlo, P. F., Salcedo, D., Onasch, T., Jayne, J. T., Miyoshi, T., Shimono, A., Hatakeyama, S., Takegawa, N., Kondo, Y., Schneider, J., Drewnick, F., Borrmann, S., Weimer, S., Demerjian, K., Williams, P., Bower, K., Bahreini, R., Cottrell, L., Griffin, R. J., Rautiainen, J., Sun, J. Y., Zhang, Y. M. and Worsnop, D. R.: Ubiquity and dominance of oxygenated species in organic aerosols in anthropogenically-influenced Northern Hemisphere midlatitudes, Geophys. Res. Lett., 34(13), L13801, doi:10.1029/2007GL029979, 2007.

Zhang, X., Knochenmuss, R., Siems, W. F., Liu, W., Graf, S. and Hill, H. H.: Evaluation of Hadamard Transform Atmospheric Pressure Ion Mobility Time-of-Flight Mass Spectrometry for Complex Mixture Analysis., Anal. Chem., 86(3), 1661–70, doi:10.1021/ac403435p, 2014.

Zhao, Y., Kreisberg, N. M., Worton, D. R., Teng, A. P., Hering, S. V. and Goldstein, A. H.: Development of an In Situ Thermal Desorption Gas Chromatography Instrument for Quantifying Atmospheric Semi-Volatile Organic Compounds, Aerosol Sci. Technol., 47(3), 258–266, doi:10.1080/02786826.2012.747673, 2013.

Appendix A: List of Compounds Compared

Compounds compared between the A-CIMS, I-CIMS, and TAG. Molecular formulas were identified in the two CIMS instruments, and compounds were identified in the TAG. See main text for detailed interpretation.

Molecular Formula	Likely Compound	C* Value	Source
$C_5H_8O_5$	Hydroxy glutaric acid	0.21	(Bilde and Pandis, 2001)
$C_9H_{14}O_4$	Pinic acid	10	(Bilde and Pandis, 2001)
$C_{10}H_{16}O_3$	Pinonic acid	1000	(Müller et al., 2012)

Possible compounds compared between the A-CIMS and the PTRMS, identified by their molecular formula. The possible compound is one of many possible isomers.

Molecular Formula	Possible Compound
$C_{10}H_{20}O_2$	Decanoic acid
$C_{17}H_{34}O_2$	Heptadecanoic acid
$C_{12}H_{24}O_2$	Lauric acid
$C_4H_6O_3$	Methacrylic acid epoxide
$C_{14}H_{28}O_2$	Myristic acid
$C_9H_{18}O_2$	Nonanoic acid
$C_{16}H_{32}O_2$	Palmitic acid
$C_{15}H_{30}O_2$	Pentadecanoic acid
$C_8H_{16}O_2$	Valproic acid

Appendix B: Average Conditions at SOAS

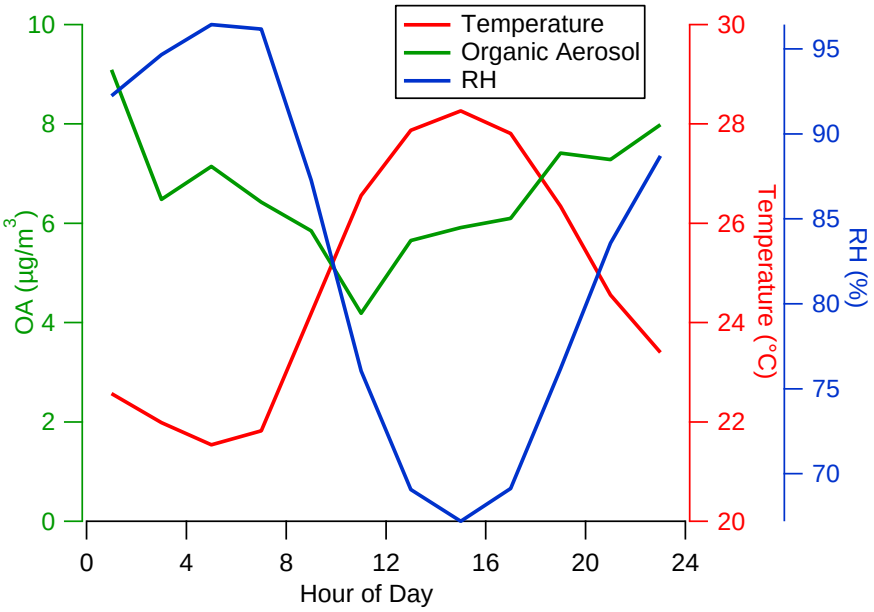

Average diurnal cycle over the 9-day period of organic aerosol concentration, temperature and relative humidity.